

**CHARACTERIZATION OF MONOLITHIC ACTIVE
PIXEL SENSORS (MAPS) FOR HIGH ENERGY
PARTICLE DETECTORS WITH
1-GeV ELECTRON BEAM**



Anantachai Lakrathok

**A Thesis Submitted in Partial Fulfillment of the Requirements for the
Degree of Master of Science in Physics
Suranaree University of Technology
Academic Year 2018**

การทดสอบคุณลักษณะของหัววัดชนิด Monolithic Active Pixel เพื่อตรวจจับ
อนุภาคพลังงานสูงด้วยลำอิเล็กตรอนพลังงาน 1-GeV



นายอนันตชัย ล่ากระโทก

วิทยานิพนธ์นี้เป็นส่วนหนึ่งของการศึกษาตามหลักสูตรปริญญาวิทยาศาสตรมหาบัณฑิต
สาขาวิชาฟิสิกส์
มหาวิทยาลัยเทคโนโลยีสุรนารี
ปีการศึกษา 2561

CHARACTERIZATION OF MONOLITHIC ACTIVE
PIXEL SENSORS (MAPS) FOR HIGH ENERGY
PARTICLE DETECTORS WITH
1-GeV ELECTRON BEAM

Suranaree University of Technology has approved this thesis submitted in partial fulfillment of the requirements for a Master degree.

Thesis Examining Committee



(Assoc.Prof. Dr. Sirichok Jungthawan)

Chairperson



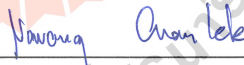
(Asst. Prof. Dr. Chinorat Kobdaj)

Member (Thesis Advisor)



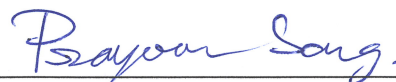
(Dr. Kritsada Kittinanapun)

Member



(Dr. Narong Chanlek)

Member



(Assoc. Prof. Dr. Prayoon Songsiriritthigul)

Member



(Assoc. Prof. Dr. Worawat Meevasana)



(Prof. Dr. Santi Maensiri)

Vice Rector for Academic Affairs
and Internationalization

Dean of Institute of Science

อนันตชัย ล่ากระโทก : การทดสอบคุณลักษณะของหัววัดชนิด Monolithic Active Pixel เพื่อตรวจจับอนุภาคพลังงานสูงด้วยลำอิเล็กตรอนพลังงาน 1-GeV

(CHARACTERIZATION OF MONOLITHIC ACTIVE PIXEL SENSORS (MAPS) FOR HIGH ENERGY PARTICLE DETECTORS WITH 1-GeV ELECTRON BEAM)

อาจารย์ที่ปรึกษา : ผู้ช่วยศาสตราจารย์ ดร.ชิโนรัตน์ กอบเดช, 74 หน้า

มหาวิทยาลัยเทคโนโลยีสุรนารีและสถาบันวิจัยแสงซินโครตรอน ได้ร่วมมือเพื่อติดตั้งและพัฒนาชุดประกอบของเซนเซอร์แบบพิกเซลที่สถานีทดสอบด้วยลำอิเล็กตรอนเพื่อทดสอบคุณลักษณะของเซนเซอร์ที่จะถูกติดตั้งในหัววัดขั้นสูงสุดในสถานีทดลองการชนไอออนหนัก องค์การวิจัยนิวเคลียร์ยุโรป โดยการใช้เทคโนโลยีของเซนเซอร์แบบ Monolithic Active Pixel เพื่อสร้างเซนเซอร์ที่มีคุณสมบัติสูญเสียพลังงานลดทอนต่ำจากการวิ่งผ่านของอนุภาค ประสิทธิภาพการตรวจวัดสูง มีความละเอียดในการวัดตำแหน่งการชนสูง และมีระบบการอ่านค่าทางอิเล็กทรอนิกส์ที่รวดเร็ว โดยใช้หัววัดนี้เรียกว่า ALICE pixel detector หรือ ALPIDE เซนเซอร์ที่ถูกนำมาเรียงกัน 7 ชั้นเรียกว่า Telescope ได้ถูกติดตั้งเพื่อทดสอบคุณลักษณะของเซนเซอร์ ALPIDE ด้วยลำอิเล็กตรอนพลังงาน 1-GeV ที่สถานีทดสอบด้วยลำอิเล็กตรอน สถาบันวิจัยแสงซินโครตรอน โดยเซนเซอร์ที่ต้องการทดสอบคุณสมบัติถูกติดตั้ง (Device Under Test) ไว้ตรงกลางของทั้ง 7 แผ่นที่ถูกเรียงไว้ โดยคุณลักษณะของเซนเซอร์ ALPIDE ถูกทดสอบภายใต้เงื่อนไขการเปลี่ยนแปลงของค่าจำนวนกลุ่มที่ลำอิเล็กตรอนทะลุผ่านแผ่นเซนเซอร์ที่ต้องการทดสอบคุณสมบัติ จากการทดสอบได้แสดงคุณลักษณะของหัววัดชนิดนี้ว่าขนาดของกลุ่มของลำอนุภาคที่วิ่งผ่านเซนเซอร์เฉลี่ย ณ 1.98 เม็ดพิกเซลที่ค่าจำนวนกลุ่มที่ลำอิเล็กตรอนทะลุผ่านแผ่นเซนเซอร์ที่แตกต่างกันและประสิทธิภาพการตรวจวัดอนุภาคของเซนเซอร์นี้มีค่ามากกว่าร้อยละ 99 ของการตรวจวัดซึ่งบรรลุเป้าหมายของคุณสมบัติการออกแบบเซนเซอร์ชนิดนี้

สาขาวิชาฟิสิกส์
ปีการศึกษา 2561

ลายมือชื่อนักศึกษา อนันตชัย ล่ากระโทก

ลายมือชื่ออาจารย์ที่ปรึกษา ชิโนรัตน์ กอบเดช

ลายมือชื่ออาจารย์ที่ปรึกษาร่วม อนุชา สิงห์รัมย์

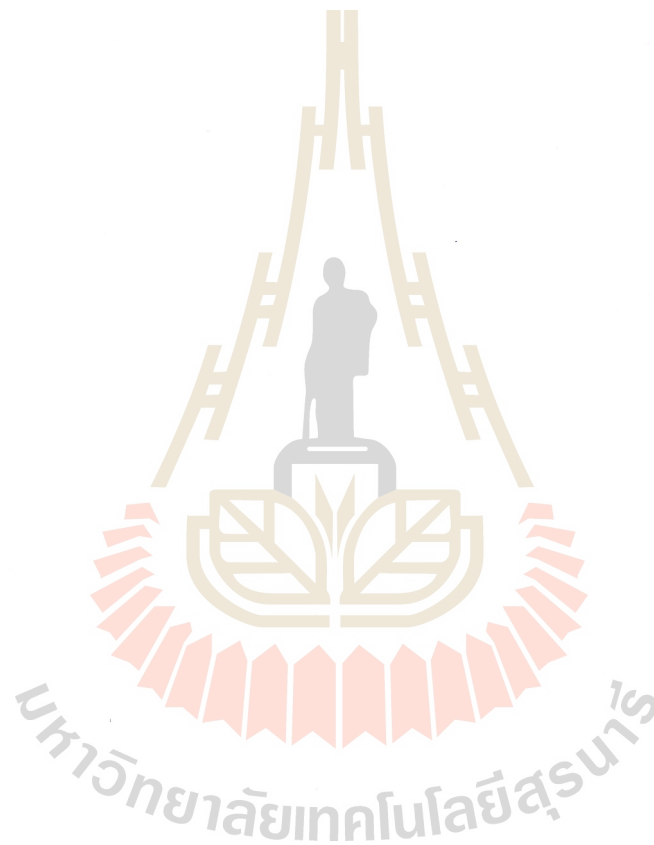
ลายมือชื่ออาจารย์ที่ปรึกษาร่วม ดวงอ๋อ จันทร์แก้ว

ANANTACHAI LAKRATHOK : CHARACTERIZATION OF
MONOLITHIC ACTIVE PIXEL SENSORS (MAPS) FOR HIGH
ENERGY PARTICLE DETECTORS WITH 1-GeV ELECTRON BEAM
THESIS ADVISOR : ASST. PROF. CHINORAT KOBDAJ, Ph.D.
74 PP.

A LARGE ION COLLIDER EXPERIMENT/MONOLITHIC ACTIVE PIXEL
SENSOR/ALICE PIXEL DETECTOR SENSOR/ SYNCHROTRON LIGHT
RESEARCH INSTITUTE-BEAM TEST FACILITY/DEVICE UNDER
TEST/TELESCOPE/NUMBER OF CLUSTER OF DUT/DETECTION
EFFICIENCY

Suranaree University of Technology (SUT) and Synchrotron Light Research Institute (SLRI) have collaborated on setting up and development of a Pixel sensor telescope at SLRI Beam Test Facility (BTF) for characterization of a sensor that will be used for the Inner Tracking System of A Large Ion Collider Experiment (ALICE), CERN. The Monolithic Active Pixel sensor (MAPS) technology is used to fabricate a sensor with low-material budget, high detection efficiency, high spatial resolution and faster read-out electronics. It is called the ALICE Pixel detector or ALPIDE sensor. The seven planes of ALPIDE sensors, which is called a Telescope, is set up for sensor characterization with 1 GeV/c electron beam at SLRI-BTF. The interested sensor or a device under test (DUT) placed in a middle of a telescope is characterized with variation of the number of cluster of electrons.

The results show that the average cluster size is 1.98 pixels, and ALPIDE detection efficiency is over 99 % which is meeting with the upgraded requirement.



School of Physics

Academic Year 2018

Student's Signature Anantachai Iakrathok

Advisor's Signature C. Kobdaj

Co-advisor's Signature Kater Ulayn

Co-advisor's Signature Nirong Anurak

ACKNOWLEDGEMENTS

I would like to express my gratitude to the following people for their encouragement, assistance, and support which have enabled me to complete my thesis. My deepest appreciation goes first and foremost to my thesis advisor Asst. Prof. Dr. Chinorat Kobdaj and My thesis co-adviser Dr.Kritsada Kittimanapun and Dr. Narong Chanlek from Synchrotron Light Research Institute (SLRI), Thailand for their great support in experimental, patient guidance, consideration, and assistance throughout the study. Without their help, this work would not be possible for success. I would like to thank Assoc. Prof. Dr. Prayoon Songsiriritthigul, Assoc. Prof. Dr. Sirichok Jungthawan for whom being member of the thesis committee and giving me excellent advice.

I would also like to thank all lecturers in the School of Physics, who have taught me and made it possible the expansion of my knowledge and my professional development in the past three academic years. Many thanks are for our group members, especially Mr.Natthawut laojamngongwong, Mr.Wanchaloem Poonsawat, for those valuable discussions and fruitful suggestions and WP5 ALICE team including Magnus Meger, Jacobus Willem Van hoorne, Felix Reidt and Monika Korafago who develop and work hard for an ALPIDE sensor. They provide various advice that pressures me to solve many problem during I did experiment. I would like to big thank SLRI scholarship for financial support during my master degree.

Last but not least, I would like to extend my immense gratitude to my parents for their continuous love, understanding, encouragement and support throughout the progress and for motivating me to complete my study.

Anantachai Lakrathok



CONTENTS

	Page
ABSTRACT IN THAI	I
ABSTRACT IN ENGLISH	II
ACKNOWLEDGEMENTS	IV
CONTENTS	VI
LIST OF TABLES	IX
LIST OF FIGURES	X
LIST OF ABBREVIATIONS	XIV
CHAPTER	
I INTRODUCTION	1
II BACKGROUND KNOWLEDGE	9
2.1 Interaction of particles in matter	9
2.1.1 Radiation interaction in matter	9
2.1.2 The charged massive particles passage in material	9
2.1.3 Massive particles mean energy loss in matter	10
2.1.4 Radiation length	13
2.1.5 Multiple coulomb scattering	14
2.2 Monolithic Active Pixel Sensor (MAPS)	15
2.3 ALPIDE principle	16

CONTENTS (Continued)

	Page
III SYNCHROTRON LIGHT RESEARCH INSTITUTE-BEAM	
TEST FACILITY (SLRI-BTF)	20
3.1 Electron Beam Telescope setup	22
IV DATA TAKING AND ANALYSIS FRAMEWORK	26
4.1 Test beam framework	26
4.1.1 Eudaq framework	26
Data Taking	26
Online Monitor	28
4.1.2 Data analysis Framework (EUtelescope)	29
Converter	29
DeadColumn	33
Hotpixel	33
Clustering	35
Hitmaker	35
Pre-Alignment	35
Alignment	36
Fitter	36
Analysis	37
Average cluster size	38
Detection efficiency	38
Geometry Application Programming Interface for Re- construction (GEAR) file	39

CONTENTS (Continued)

	Page
V RESULT AND DISCUSSION	40
5.1 Test beam commission	40
5.2 Test beam data analysis	40
5.2.1 Beam data modification in case of a problem	41
5.2.2 Modification	44
5.3 Relation of high intensity beam	44
5.4 Discussion	49
VI CONCLUSION	50
REFERENCES	52
APPENDICES	
APPENDIX A SLRI ACCELERATOR	57
Magnetic setting for Beam Test Facility station	61
APPENDIX B EXTENSION OF AN OPERATION MANUSCRIPT FOR AN EUDAQ FRAMEWORK	66
Configuration	66
EUDAQ restarting in case of trouble	68
APPENDIX C FUNCTIONAL TEST	70
CURRICULUM VITAE	74

LIST OF TABLES

Table		Page
1.1	The new ITS pixel sensor requirements (Abelev et al., 2014).	5
1.2	Four prototype sensors from Towerjazz (Mager, 2016)(Abelev et al., 2014).	5
3.1	Electron Beam Parameters at High-energy Beam Transport Line (HBT) (Kittimanapun et al., 2016).	23
5.1	Results for good run before analysis modification.	46
5.2	List of run data in case of problem during analysis.	47
A.1	Settings of Synchrotron booster magnet power supply.	62
A.2	Settings of High-energy Beam Transport(HBT) line magnet power supply for a point beam profile.	63
A.3	Settings of High-energy Beam Transport(HBT) line magnet power supply for a full beam profile.	65



LIST OF FIGURES

Figure		Page
1.1	An ALICE experiment structure (ALICEwebsite, 2019).	1
1.2	New ITS at LS2 2018/2019 (Abelev et al., 2014).	3
1.3	A new ITS cross-section at LS2 2018/2019 (Mager, 2016).	4
1.4	The ALPIDE family prototypes and their goals (Willem van Hoorne, 2015).	7
1.5	ALPIDE chip sensing area (M.Luciano ITS report 8th ITS upgrade and O2 workshop, 2017).	8
2.1	The relation of a positive muon incoming speed with a stopping power in Cu matter and Bethe-Bloch formula demonstration (Beringer et al., 2012).	13
2.2	the layout of a multiple coulomb scattering process in high thickness matter with an incoming particle's passage.	15
2.3	A cross-section of Towerjazz Monolithic Active Pixel Sensor (MAPS) (Mager, 2016).	16
2.4	Architecture of the ALPIDE chip.	18
2.5	Block diagram of an ALPIDE pixel (Keil, 2017).	19
3.1	Target manipulator for controlling amount of an electron.	21
3.2	Beam Test station layout at Synchrotron Light Research Institute Beam Test Facility.	21
3.3	Synchrotron Light Research Institute Beam Test facility layout.	22

LIST OF FIGURES (Continued)

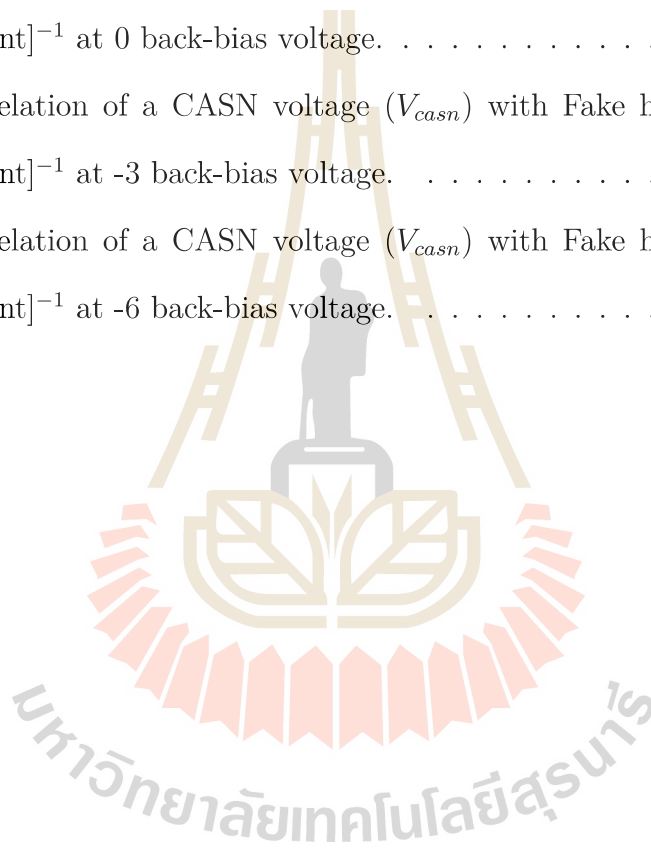
Figure		Page
3.4	A diagram of telescope component, there are a real instrument (A) and a telescope graphic (B).	24
3.5	A diagram of telescope structure.	25
4.1	The EUDAQ framwork window, there are the run control, the log window, the data collector and the pALPIDEfs producers.	27
4.2	Raw hit-map for showing up an collective hit position contour plot on each sensor.	30
4.3	Position correlation plots for position on x and y axis of plane 0 with nearby plane(plane 1) and other couple (plane 0 with plane 2) to plane 0 with plane 6 respectively.	31
4.4	The relation of a Device Under Test (DUT) number of cluster with a hit of any number of cluster.	32
4.5	The relation of a sensor type in the telescope with an average hit of any sensor type.	32
4.6	The relation of an event for a telescope with 7 plane hit of sensor.	33
4.7	The flowchart of the EuTelescope working procedure adapted from M.korafago.	34
4.8	Track fitting procedure on multiple plane adapted from M.korafago.	37
4.9	Cluster size layout that performs on a Monolithic active pixel sensor with a particle track.	38

LIST OF FIGURES (Continued)

Figure		Page
5.1	Hitmap from reference frames of a telescope.	41
5.2	Correlation plots of x axis on plane 0 with plane 1, 2, 3, 4, 5 and 6; plane 1 with plane 2; plane 2 with plane 3; plane 3 with plane 4; and plane 4 with plane 5, respectively.(ordering from left to right and top to bottom) from a reference frame of a telescope.	42
5.3	Correlation plots of y axis on plane 0 with plane 1, 2, 3, 4, 5 and 6; plane 1 with plane 2, plane 2 with plane 3; plane 3 with plane 4; and plane 4 with plane 5, respectively.(ordering from left to right and top to bottom) from a reference frame of a telescope.	43
5.4	Flowchart of an Eutelescope working procedure adapted from M.korafago.	45
5.5	Relation of the cluster size of an ALPIDE chip (unit in a number of pixel) with the number of cluster of DUT.	48
5.6	Relation of Detection efficiency with a number of cluster of DUT.	49
A.1	An Electron gun at Synchrotron Light Research Institute.	58
A.2	A Linear Accelerator (LINAC) at Synchrotron Light Research In- stitute.	58
A.3	Synchrotron booster at Synchrotron Light Research Institute.	59
A.4	High-energy Beam Transport at Synchrotron Light Research Insti- tute.	61
A.5	An electron point beam profile.	64
A.6	An electron full beam profile.	64

LIST OF FIGURES (Continued)

Figure		Page
C.1	a relation of threshold current(I_{thre}) with Fake hit rate [pixel · event] ⁻¹ at 0, -3 ,-6 back-bias voltage.	71
C.2	a relation of a CASN voltage (V_{casn}) with Fake hit rate [pixel · event] ⁻¹ at 0 back-bias voltage.	72
C.3	a relation of a CASN voltage (V_{casn}) with Fake hit rate [pixel · event] ⁻¹ at -3 back-bias voltage.	73
C.4	a relation of a CASN voltage (V_{casn}) with Fake hit rate [pixel · event] ⁻¹ at -6 back-bias voltage.	73



LIST OF ABBREVIATIONS

ALICE	A Large Ion collider experiment
ALPIDE	ALICE Pixel detector
MAPS	Monolithic Active Pixel Sensor
QGP	Quark Gluon Plasma
SLRI	Synchrotron Light Research Institute
pALPIDEfs	prototype ALPIDE Pixel detector full-scale
BTF	Beam Test Facility
GeV	Giga electron-volts
CMOS	Complementary metal-oxide-semiconductor
DUT	Device Under Test
LINAC	Linear Accelerator
LBT	Low-energy Beam Transport
HBT	High-energy Beam Transport
lcio	linear collider input/output
QCD	Quantun-Chromo Dynamics
GEAR	Geometry description
I_{thr}	Threshold current
V_{casn}	CASN voltage
FIFO	First-In First-Out

LIST OF ABBREVIATIONS (Continued)

SCANDACS	Scan Digital to Analogs Converter Scanning
LHC	Large Hadron collider
ITS	Inner Tracking System
TPC	Time-Projection Chamber
MFT	Muon forward Tracking
HTF	Heavy Flavor Tracker
STAR	Solenoidal Tracker
RHIC	Relativistic Heavy Ion Collider
TID	Total Ionizing Dose
NIEL	Non-Ionization Energy Lose

CHAPTER I

INTRODUCTION

CERN (the European Organization for Nuclear Research) is the largest particle physics laboratory in the world. It hosts the most enormous and highest-energy particle accelerator called Large Hadron Collider (LHC). LHC consists of a 27-kilometer ring with superconducting magnets. A Large Ion Collision Experiments (ALICE) is one of the detectors at CERN. The ALICE main program is to study “the Quark-Gluon plasma (QGP)” using heavy-ion collision in the LHC. QGP is a state where quarks and gluons are not bound together on super-high matter density in infinitesimal volumes. It is believed to be the state of matter at the early time of universe. The ALICE detector can be seen in figure 1.1. with its

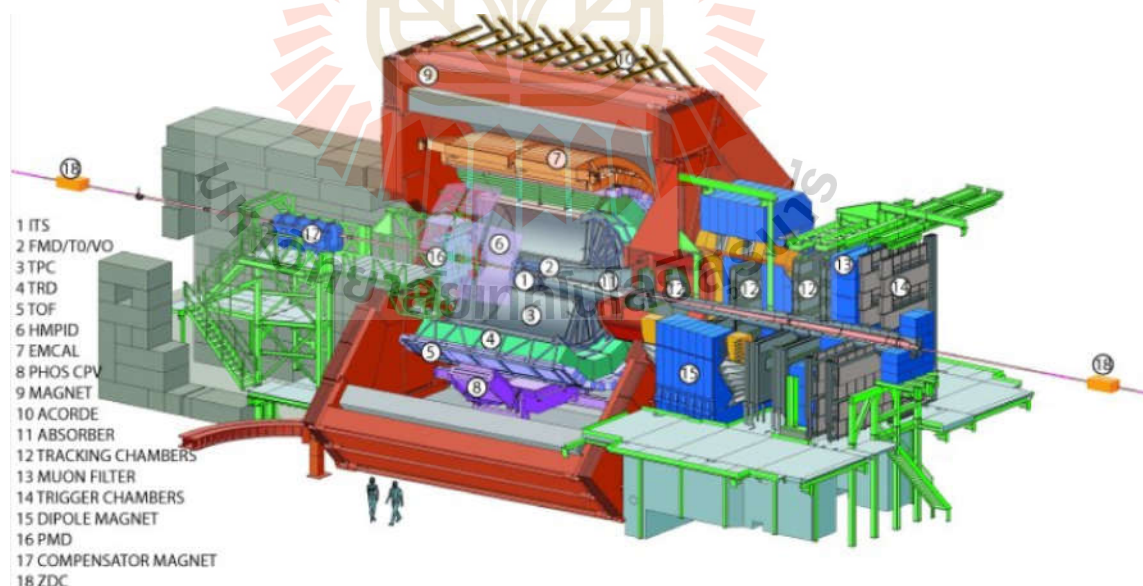


Figure 1.1 An ALICE experiment structure (ALICEwebsite, 2019).

subdetectors. (Aamodt et al., 2008) The major component are

- Tracking detector: it can be divided into the “Inner Tracking System” (ITS) and the Time-Projection Chamber (TPC). Inner tracking primary function is to do a secondary vertex reconstruction to identify and tracks a low-momentum particle and to improve an impact parameter and momentum resolution.
- Particle identification: it is used to identify a large part of many different particles and a phase space for ALICE experiment.
- Electromagnetic calorimeters: it is used to measure neutral meson, photons and to span the range from thermal emission to laborious QCD processes in the small single-arm, high-resolution and high-granularity PHOS electromagnetic calorimeter.
- Muon spectrometer: it is designed to measure the production of heavy-quark resonances with a mass resolution sufficient to separate all states.
- Forward and trigger detectors: they are designed to trigger a specialized detector system for measuring a global event characteristics. The event time is measured with good precision by a T0 detector and two sets of 12 Cherenkov counters.

An Inner Tracking System (ITS) is the closest system at a collision point. It was designed for tracking particles after the collision. The main idea of the ITS upgrade began when researchers foresaw limitations of the current ITS. Where they need to replace the existing one with a new model on the second long shut-down of LHC during 2019-2020 (LS2 LHC), see figure 1.2. By design, the new ITS consists of three inner barrels and four outer barrels. The barrels are made of a triangle structure called a “stave”. Each stave, there is a Monolithic Active

Pixel sensor (MAPS) as a main component. The idea of MAPS was first introduced into a Heavy Flavor Tracker (HFT) experiment at the Solenoidal Tracker (STAR), Relativistic Heavy Ion Collider (RHIC) in Sept 2013 (Abelev et al., 2014). Then, ALICE foresaw that it was possible to use MAPS for the new ITS as well. At that time, the ITS upgrade team was interested in using a $0.18 \mu\text{m}$ transistor. Other purposes of the ITS upgrade are to bring these sensors as close as possible to the collision point (from 33 mm down to 22 mm), to detect the short life particles (before they decay into daughter particles), and to increase their resolutions (a capability of separating the signal (real hit) from noise or fake-hits when the particle passes through the layer of sensor (Mager, 2016). From the design, the inner barrels should have a resolution less than five micrometers and the outer barrel should have resolution less than 10 micrometers. Sensor efficiency is expected to be nearly 100 % with high radiation hardness and small material budget compared to sensors that are used in the current ITS.

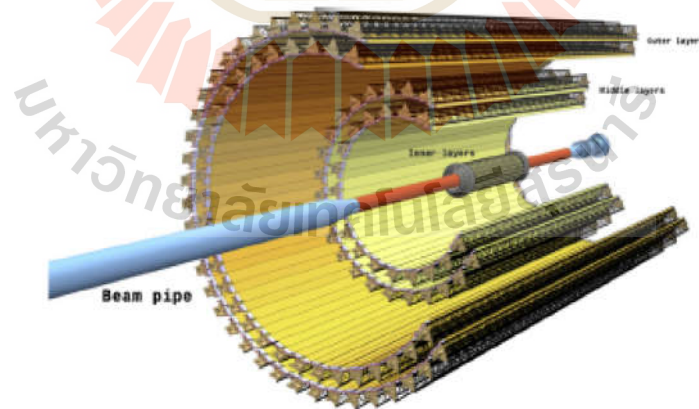


Figure 1.2 New ITS at LS2 2018/2019 (Abelev et al., 2014).

For the LHC long shut down in 2018/2019, ALICE plans to develop a new ITS and Muon forward tracking (MFT). Hence ITS developers want to provide the new ITS ability to detect the low transverse momentum of heavy-flavour hadron,

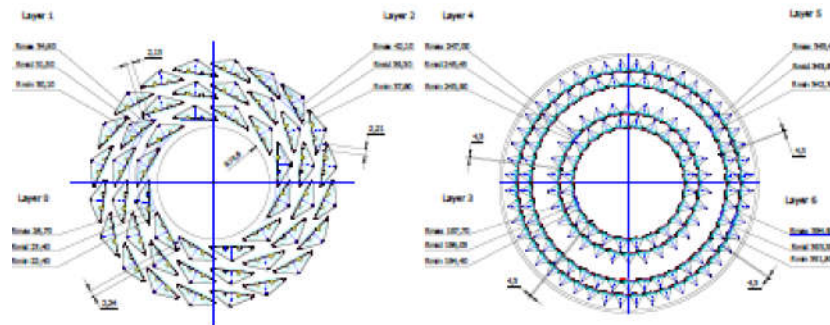


Figure 1.3 A new ITS cross-section at LS2 2018/2019 (Mager, 2016).

quarkonia, and low-mass dileptons. For the Pb-Pb collision, the detection sensitivity should be well obtained at 50 kHz (Kushpil, 2016). A development team attempted to develop a tracking sensor by using MAPS. The epitaxial layer of MAPS used in STAR RHIC, is $15 \mu\text{m}$ thick with 400Ω resistivity. From this idea, ALICE agrees to acquire properties of the new ITS (Abelev et al., 2014) as shown in Table 1.1. Therefore, ALICE had chosen “the towerjazz Complementary Metal-Oxide Semiconductor (CMOS)” technology with the transistor size of $0.18 \mu\text{m}$ since it had most parts for sensitive area and fewer peripheral circuits (Abelev et al., 2014)

Up to now, there are four candidates of MAPS that have been considered for the new ITS upgrade, MISTRAL, ASTRAL, CHERWELL and ALPIDE. Details of four candidates (Mager, 2016)(Abelev et al., 2014) are shown in Table 1.2. Finally, ALICE had chosen to use ALPIDE because it has shortest integration time and lowest power consumption (ALICE ITS upgrade collaboration, 2016). Historical development of ALPIDE started from Explorer 0. The forward generations are designed and developed for corresponding an upgrade requirements. The newer generations were Explorer-1 for study an epitaxial layer properties. An pALPIDEss-0 for verification in-matrix sparsification, front-end circuit verification ,and first variant of an ALPIDE architecture in Mar, 2013. Jan 2014,

Table 1.1 The new ITS pixel sensor requirements (Abelev et al., 2014).

Parameter	Inner barrel	Outer barrel
Max. silicon thickness	50 μm	
Intrinsic spatial resolution	5 μm	10 μm
Chip size	15 mm x 30mm (r ϕ \times z)	
Max. dead area on chip	2 mm (r ϕ), 25 μm (z)	
Max. power density	300 $\frac{\text{mW}}{\text{cm}^2}$	100 $\frac{\text{mW}}{\text{cm}^2}$
Max. integration time	30 μs	
Max. dead time	10% at 50 kHz Pb-Pb	
Min. detection efficiency	99%	
Max. fake hit rate	10^{-5} [pixel \cdot event] $^{-1}$	
TID radiation hardness	700 krad	10 krad
NIEL radiation hardness	10^{13} 1 MeV $n_{\text{eq}}/\text{cm}^2$	3×10^{10} 1 MeV $n_{\text{eq}}/\text{cm}^2$

Table 1.2 Four prototype sensors from Towerjazz (Mager, 2016)(Abelev et al., 2014).

Architecture (Discriminator, read out)	Pitch (r ϕ \times z) (μm^2)	Integration time (μs)	Power consumption (mW/cm 2)
MISTRAL (end-of-column, rolling-shutter)	22 \times 33.3	30	200
ASTRAL (in-pixel, rolling-shutter)	36 x 31	20	60
CHERWELL (in-strixel, rolling-shutter)	20 x 20	30	90
ALPIDE (in-pixel, in-matrix sparsification)	28 x 28	4	<50

an Investigator-0 was represented for Charge-collection time measurement, Pixel-pitch, an electrode-geometry studies, 135 mini-matrices, and Parallel analogue output. A pALPIDEss-1 was planned to front-end optimizations and variations. A pALPIDE 1 was projected for exploration an On-chip bias DACs and a pad-over matrix. Dec 2014, A pALPIDE-2 was conceived to develop a final interface except high-speed link and epitaxial layer properties. Jan 2015, A pALPIDE 3 was developed for a high-speed link evolution and a three in-pixel buffer in pixel pitch construction. The ALPIDE family informations are shown in figure 1.4.

Finally, ALPIDE (full scale) was developed and constructed which is fabricated in Sep, 2016 with the size of 15 mm \times 30 mm, 512 \times 1024 (row \times column) as shown figure 1.5. According to the Explorer-0 and Explorer-1 sensor was tested with 4 and 6 GeV/c electron beams at DESY. The results showed a detection efficiency that performs 90% to 100% of a detection efficiency (Aglieri et al., 2013). Hence it is possible to characterize an ALPIDE sensor with beam test facility at Synchrotron Light Research Institute Beam Test facility (SLRI-BTF) with the electron beam energy of 1 GeV/c. The detail of an SLRI-BTF and ALPIDE telescope set up will be discussed on Chapter III. This thesis performs a characterization of the ALICE Pixel detector (ALPIDE) sensor. The sensor is tested with 1 GeV electron beam at “Synchrotron Light Research Institute Beam Test Facility (SLRI-BTF)”. The motivation and the requirement of an upgraded ITS are already given in the first part of this chapter. A related theory about this research is provided in chapter II. A detail of SLRI-BTF and Telescope setup are discussed in chapter III. A data taking and data analysis framework are described in chapter IV. The result is discussed in chapter V. A discussion and conclusion are discussed in chapter VI.

family and their goal chart.png family and their goal chart.bb

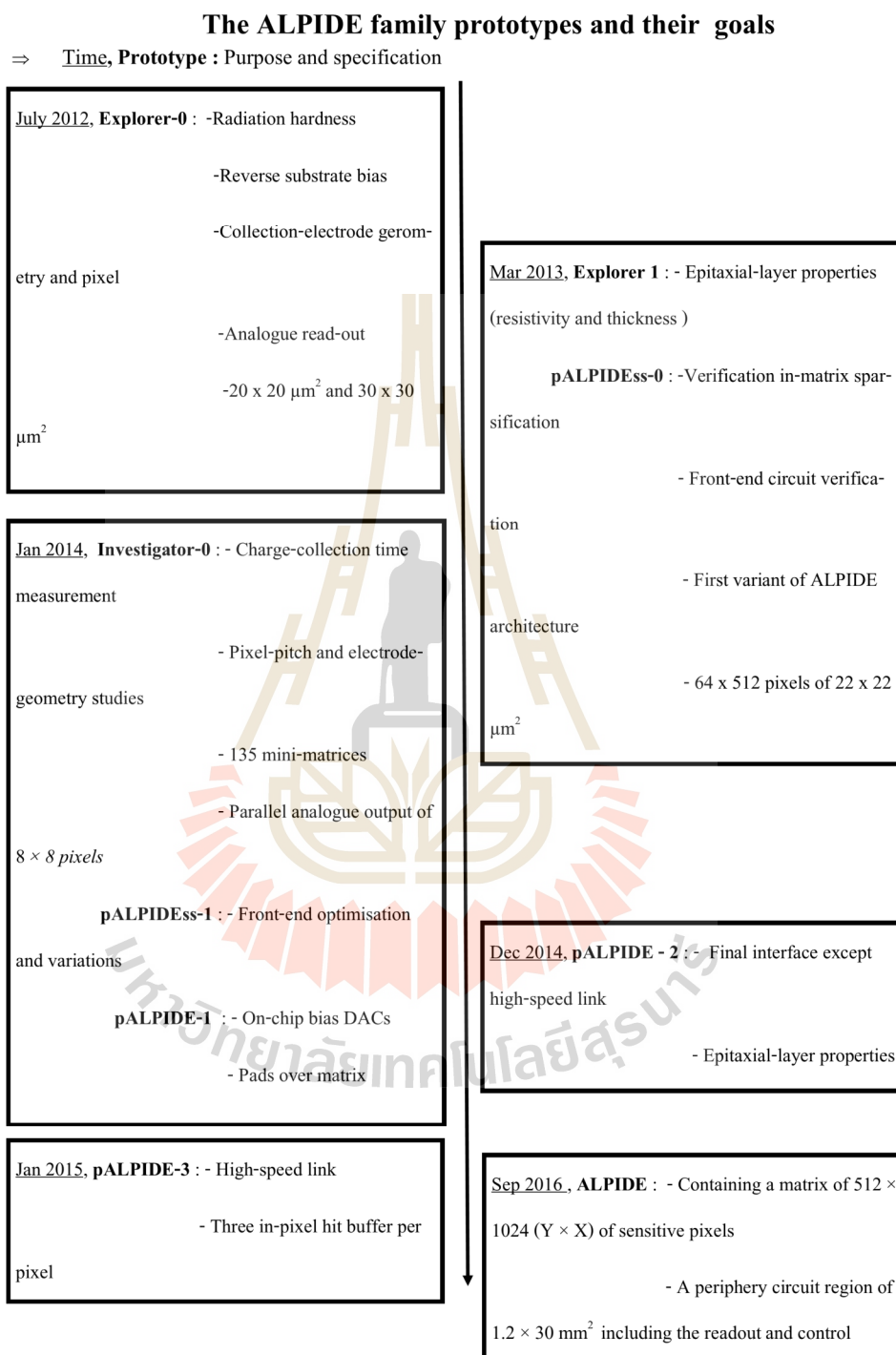


Figure 1.4 The ALPIDE family prototypes and their goals (Willem van Hoorne, 2015).

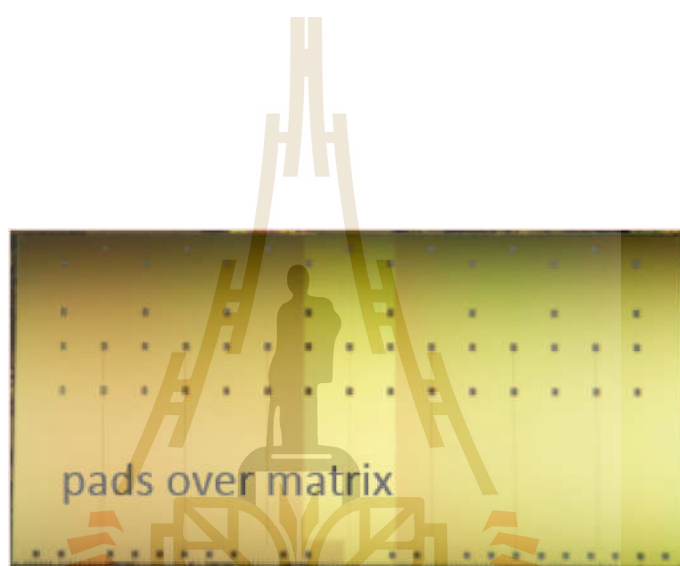


Figure 1.5 ALPIDE chip sensing area (M.Luciano ITS report 8th ITS upgrade and O2 workshop, 2017).

CHAPTER II

BACKGROUND KNOWLEDGE

2.1 Interaction of particles in matter

2.1.1 Radiation interaction in matter

When there is an radiation interaction inside the detector medium, the signal is produced in the sensing node and recorded in a read-out circuit. The interaction of the incoming particle is determined by its energy and type. Detector is mostly designed for detection an electron, a photon, an atom or molecular excitation. The detector mechanism is based on a fraction dissipation of the incoming radiation energy inside the detecting material. The radiation transfer energy spread out to generate carrier which are electron-hole pair in semi-conductor, photons in scintillation medium, and ion-pairs in a gaseous device. A read-out is obtained by collecting carriers from a detector. The important information can be obtained from a detector such as incoming particle momentum, energy ,and velocity.

2.1.2 The charged massive particles passage in material

When an incident particle interacts with electron and nuclei of matter, two main effects can be used to determine and characterize that massive charged particle. There are energy loss of a particle in a matter and deflection direction of an incident particle. The interaction mechanism depends on momentum, energy and charge of an incident particle. For example, the interaction mechanism of the

massive charged particle are (Leo, 1993),

1. Inelastic collisions with the atomic electrons of the material occur when an incoming particle collides with an orbital electron. The collision effect occur as ionization or excitation. Light charge particles are electrons or positrons which have two main contributing processes. There are ionization and bremsstrahlung.
2. Bremsstrahlung process is inversely proportional to the squared mass quantities of an incident particle.

2.1.3 Massive particles mean energy loss in matter

A stopping power is a mean energy loss per unit length. In the first half of a twenty century, the dominant collision theory is led by Hans Bethe, Bloch and other authors in 1932. The first equation that correctly describes quantum-mechanic energy loss equation in matter (Leo, 1993)(Beringer et al., 2012), since by,

$$-\frac{dE}{dx} = 2\pi N_a r_e^2 m_e c^2 \rho \frac{Z}{A} \frac{z^2}{\beta^2} \left[\ln\left(\frac{2m_e \gamma^2 v^2 W_{max}}{I^2}\right) - 2\beta^2 - \delta - 2\frac{C}{Z} \right] \quad (2.1)$$

where;

$$2\pi N_a r_e^2 m_e c^2 = 0.1535 \text{MeV} \frac{\text{cm}^2}{\text{g}}$$

$\beta = \frac{v}{c}$ of an incident particle

r_e is an electron radius (value is $2.817 \times 10^{-15} \text{m}$.)

ρ is a density of absorbing material

m_e is an electron mass

$$\gamma = \frac{1}{\sqrt{1-\beta^2}}$$

N_a is an Avogadro's number

δ is a density correction

Z is an atomic number of absorbing material

C is a shell correction

A is an atomic weight of absorbing material

I is a mean excitation potential

z is a charge of incident particle (coulomb.)

W_{max} is a maximum energy transferable in a single collision

when:

$$W_{max} = \frac{2m_e c^2 \eta^2}{1 + 2s\sqrt{1 + \eta^2 + s^2}} \quad (2.2)$$

set $s = m_e/M$ and $\eta = \beta\gamma$

The absorbing material orbital frequency (ω) is defined by mean exiting energy I which is investigated from absorbing material measurement. The last two terms of the Bethe-Bloch equation, density and shell correction, are needed to compare with experimental results. The density correction depends on an electric field which is verified with an incoming particle. The shell correction has a value when the particle velocity is close to an orbital frequency of a material boundary electron. From the relation of a positive muon momentum with its stopping power in Cu, at the low-velocity is incorrect for Bethe-Bloch description. For higher speed, the stopping power is sharply increased by $\frac{1}{\beta^2}$ factor in the equation. Until the incoming particle speed reaches $\beta = 0.96$ where the stopping power drops to a minimum value by definition as “a minimum ionizing particle” (MIP). After this. The stopping power does not increase due to the density correction effect. The radiation effect is related at ultra-speed of an incoming particle such

as a Bremsstrahlung and Cherenkov radiation. Especially, the Bremsstrahlung is dominantly occurred to be the main mechanism in case of a light particle (e.g. electron or positron). The interaction with nuclei or a target (higher atomic number particle) with an incoming light particle is a deflection and a deceleration. Hence ionization energy process sharply decreases with increasing of incoming particle energy. Nevertheless, the Bremsstrahlung radiation loss is linearly loss with increasing of incoming particle energy. In case of an electron or positron, they have a small mass by comparing with nuclei mass. So electron mostly deflects back after colliding with nuclei in a single collision. In huge number collision, they can not distinguish an electron from a positron. The maximum transferable energy should be (Meroli, 2013)(Beringer et al., 2012)

$$W_{max} = \frac{T_e}{2} \quad (2.3)$$

where: T_e is an incoming particle kinetic energy, A Bethe-Bloch equation is rearranged as,

$$-\frac{dE}{dx} = \frac{2\pi N_a r_e^2 m_e C^2 \rho Z}{A\beta^2} \left[\ln \frac{\tau^2(\tau+2)}{2\left(\frac{I}{m_e C^2}\right)^2} + F^{+-}(\tau) - \delta - 2\frac{C}{Z} \right] \quad (2.4)$$

when;

$$\tau = \frac{T_e}{m_e C^2} \quad (2.5)$$

and the positive term for positron:

$$F^+(\tau) = 2\ln 2 - \frac{\beta^2}{12} \left(23 + \frac{14}{\tau+2} + \frac{10}{(\tau+2)^2} + \frac{4}{(\tau+2)^3} \right) \quad (2.6)$$

also the negative term for electron:

$$F^-(\tau) = 1 - \beta^2 \left(\frac{\tau^2}{8} - \frac{(2r_e + 1)\ln 2}{(\tau+1)^2} \right) \quad (2.7)$$

where, r_e is an electron radius (value is 2.817×10^{-15} m.)

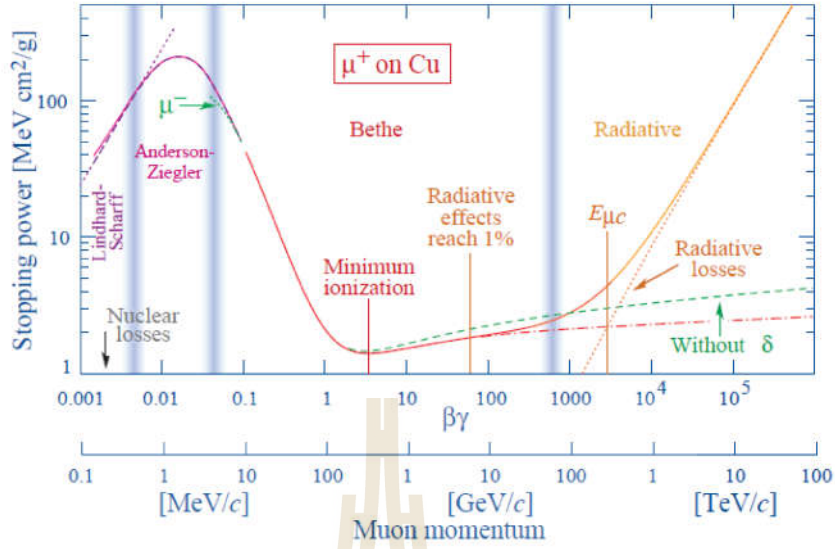


Figure 2.1 The relation of a positive muon incoming speed with a stopping power in Cu matter and Bethe-Bloch formula demonstration (Beringer et al., 2012).

$\beta = \frac{v}{c}$ of an incident particle, m_e is an electron mass, c is a speed of light

2.1.4 Radiation length

The bremsstrahlung radiation and electron-positron pair production are commonly generated from electromagnetic cascade by a charged particle through matter. The significant heavy charged particles produce more electromagnetic cascade than light charged particles. The average passage which generates bremsstrahlung radiation and electron-positron pair production is called the radiation length X_0 that is represented in common unit $\frac{\text{g}}{\text{cm}^2}$. Therefore, the energy loss is related to a scaling variable. It can be presented in form of a radiation length (Leo, 1993) as equation

$$\frac{dE}{dx} = \frac{1}{X_0} E \longrightarrow E(t) = E_0 e^{-\frac{t}{X_0}} \quad (2.8)$$

where E_0 : initial energy of the incident particle. The most case, it is presented in a high energy photon for $7/9X_0$ of a probability where occur an electron-positron pair production. While high energy electron loses $1/e$ of its initial energy by bremsstrahlung radiation, an atomic number is the primary variable that determines a radiation length as shown in a useful approximation form are (Tsai, 1974),

$$X_0 = 716.4 \frac{A}{Z(Z+1) \ln \frac{287}{\sqrt{Z}}} \quad (2.9)$$

2.1.5 Multiple coulomb scattering

Whenever charged particles collide with nuclei, it will be changed a small trajectory direction. The small angle is deviated by statistic random as a zig-zag trajectory. A thickness of a matter can contribute to situation of a coulomb scattering (Meroli, 2013)(Beringer et al., 2012).

1. Single scattering is considered under an ultra tiny matter thickness. The Rutherford scattering formula can be described by,

$$\frac{d\sigma}{d\omega} = \left(\frac{1}{4\pi\epsilon_0}\right)^2 \frac{z^2 e^4}{M^2 C^4 \beta^4} \frac{1}{\sin^4(\Theta/2)} \quad (2.10)$$

2. Plural scattering is considered under a few ten-coulomb interactions of more thick matter.
3. Multiple scattering is investigated at a very thick matter. Coulomb interaction is performed in a large number. The statistic can be shown up by angular dispersion under the Gaussian model distribution.

$$\Theta_0 = \frac{13.6}{\beta c p} z \sqrt{x/X_0} [1 + 0.038 \ln(x/X_0)] \quad (2.11)$$

After particle passing through material, 98 % concentration of incoming

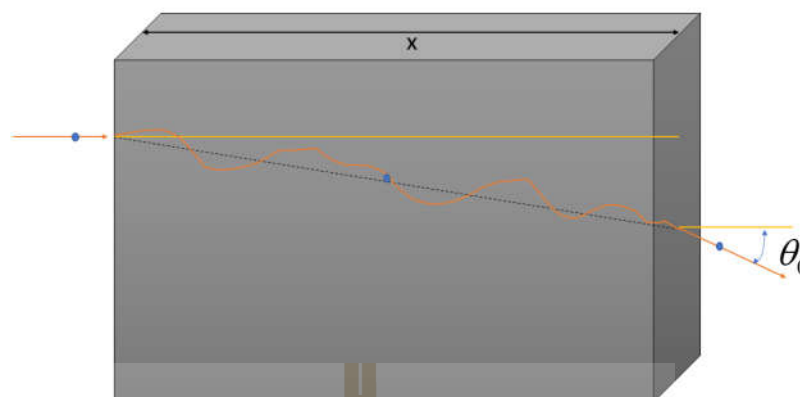


Figure 2.2 the layout of a multiple coulomb scattering process in high thickness matter with an incoming particle's passage.

beam is diverged to θ_0 at x thickness of a matter, θ_0 is projection of an angle θ on a plane which is equal to $\theta_0 = \frac{\theta}{\sqrt{2}}$

2.2 Monolithic Active Pixel Sensor (MAPS)

“Monolithic Active Pixel Sensor (MAPS)” is a combination of a sensing layer with an electronic read-out on a layer for reducing a material budget (less thickness) and large charge collection. There are N-well diode, P-well, P-MOS transistor, N-MOS transistor, and Deep p-well. The function of an N-well diode is to keep ionized electrons that generate from ionization. P-well is used for producing depletion region to distinguish the ionized electrons from a background. The NMOS-transistor and the P-MOS transistor are the electronic circuits located on top of the sensor used as Analog to Digital signal Converter (ADC) and logic gate. The deep P-well is designed to shield PMOS and NMOS-transistor from leaking electron. For MAPS operation, also back-bias voltage ($V_{back-bias}$) is applied to generate the depletion region for keeping out the background electron in the

medium (Snoeys, 2014) as shown in figure 2.3. Whenever high-energy particles

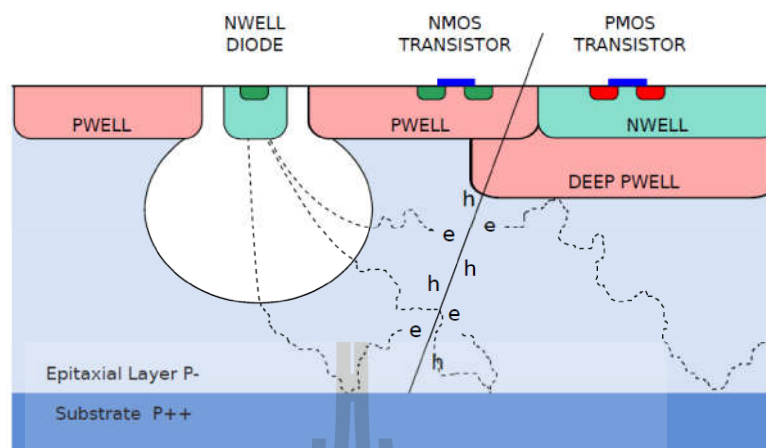


Figure 2.3 A cross-section of TowerJazz Monolithic Active Pixel Sensor (MAPS) (Mager, 2016).

pass through an epitaxial layer (in silicon die in MAPS or sensitive volume), they ionize and generate electron-hole pairs in the epitaxial layer. The wafer is doped for high resistivity ($> 1\text{k}\Omega \cdot \text{cm}$) to reduce charge carrier trapping in silicon layer (making a charge losing in an electronics read-out) with a sufficient radiation tolerance. Then electrons from ionization move as random motion (non-steady moving direction) by diffusion until they reach at the depletion region where there exist electric field to induce electron movement toward the N-well diode. Whenever particles pass through a silicon die, an incoming particle always lose the energy from ionization.

2.3 ALPIDE principle

The ALICE Pixel Detector (ALPIDE) sensor is designed for a new Inner Tracking System (ITS) and constructed by using CMOS Monolithic Active Pixel technology. The ALPIDE chip is measured 15 mm (width) \times 30 mm (length) and contains a matrix of 512×1024 pixels, (width \times length) $29.24\ \mu\text{m} \times 26.88\ \mu\text{m}$

for any pixel as shown in figure 2.4. A peripheral circuits of $1.2 \text{ mm} \times 30 \text{ mm}$ includes the control and read-out functionality (Keil, 2017). In each pixel, there are a sensing node, a front-end amplifying and shaping stage, a discriminator and a digital section. A digital sector consists of three-hit storage registers (Multi-Event Buffer or MEB), pulsing logic, and a pixel masking register. A front-end and discriminator continuously operate and characterize a non-linear response. Their transistors are biased in weak inversions with the power consumption about 40 nW. For a front-end output, there is an order of $2 \mu\text{s}$ of a peaking time. A discrimination pulse had a $10 \mu\text{s}$ of a typical duration time. A global STROBE signal can be used to control a discriminated hit in a storage register. A STROBE is pushed to the selected cell whenever the front-end is over a threshold. A pixel hit is sent into one of three in-pixel memory cells. The common STROBE signal are produced from the peripheral circuit. The STROBE signal is used to control the storage of the pixel hit information in the pixel event buffers. An external command (TRIGGER) can trigger a level of the internal STROBE signal, but an internal sequencer can optionally initiate the internal STROBE signal. Because the duration of the STROBE signal can program, a pulse injection capacitor is constructed for test charge injection in the input of the front-end for all pixel. A digital-only pulsing mode is also available to force the logic writing in the pixel memory cells. The pulsing patterns are entirely able to program. The readout of pixel hit data named Priority Encoder from the matrix which consists of 512 instances of this circuit. There is one circuit for every two-pixel columns. The Priority Encoder performs the first-pixel periphery address with a hit in its double column and selects a pixel according to a hardwired topological priority. A hit on a pixel is chosen during a hit transfer cycle. A pixel address is provided and transmitted to the periphery circuit, and the in-pixel memory element is finally

reset (ALICE ITS upgrade collaboration, 2016).

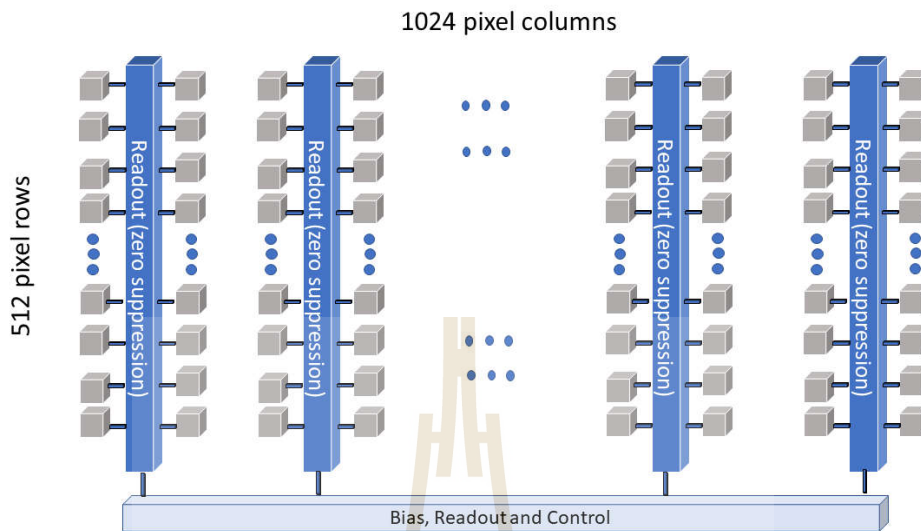


Figure 2.4 Architecture of the ALPIDE chip.

The next chapter gives a detail of Synchrotron Light Research Institute-Beam Test Facility, beam parameter and telescope setup.

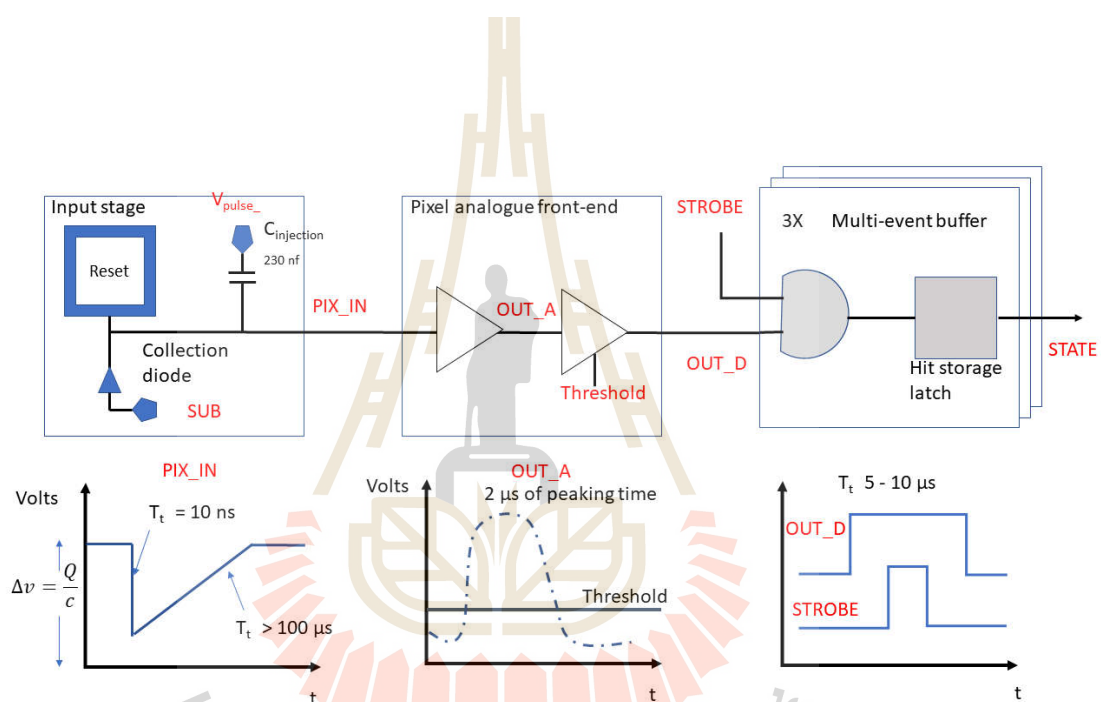


Figure 2.5 Block diagram of an ALPIDE pixel (Keil, 2017).

CHAPTER III

SYNCHROTRON LIGHT RESEARCH INSTITUTE-BEAM TEST FACILITY (SLRI-BTF)

Synchrotron Light Research Institute-Beam Test Facility (SLRI-BTF) station is a experimental station providing 1 GeV electron beam service for testing an equipment. SLRI-BTF is separated into three parts

1. Electron source: produce an electron beam from an electron gun, make bunch from a buncher, accelerate to 40 MeV of energy by the Linear accelerator, and transport to the synchrotron booster by the low energy transport line.
2. Beam reduction:a tungsten manipulator is used to control amount of electron. It is placed at the end of the low energy transport line. The amount of electrons depends on a depth of a target which is control by a servo motor as shown in figure 3.1.
3. Electron beam test station:a sample can be bombarded by an electron beam on this station to characterize a sample properties with electron beam. For example, a sample is the ALPIDE chip. The ALPIDE chips are assembled to be a 7-layer of sensors for characterization. The electron beam is released from electron pipe and passes through a TimePix Silicon detector that is set as a beam checking sensor for checking an incoming electron beam before reaching a telescope as figure 3.2.



Figure 3.1 Target manipulator for controlling amount of an electron.



Figure 3.2 Beam Test station layout at Synchrotron Light Research Institute Beam Test Facility.

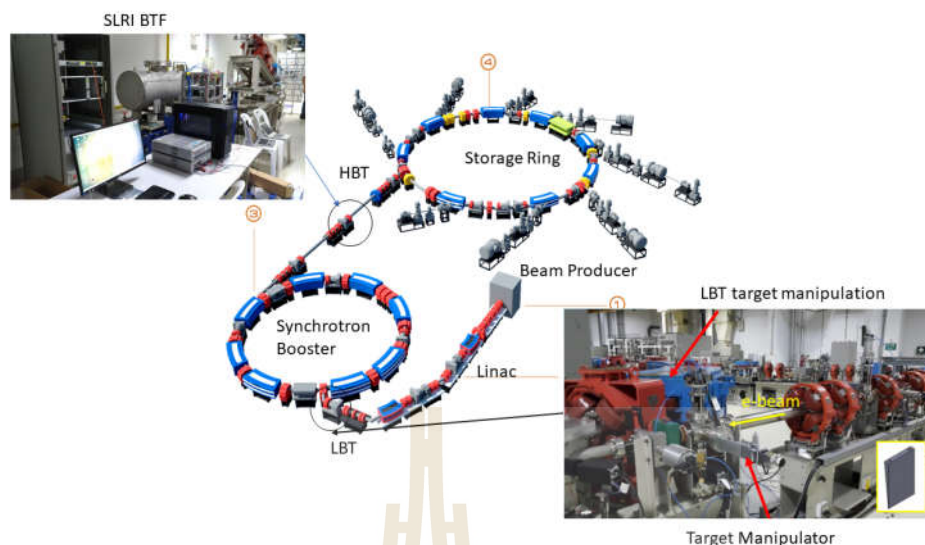


Figure 3.3 Synchrotron Light Research Institute Beam Test facility layout.

There are two periods of service, after morning injection (9 a.m.) and night injection (9 p.m.) of electron beam for a storage ring. SLRI-BTF can provide 8-10 hrs. at 0.5 Hz of a repetition rate. To focus the beam, a quadrupole magnet, dipole magnet, octa-pole are used to bend and compose an electron beam for beam profile adjustment at the High-energy Beam Transport line (HBT) by the HBT beam properties as shown in table 3.1.

3.1 Electron Beam Telescope setup

The telescope consists of multiple planes of sensor, which is 7-planes in our case, to perform a sensor characterization at the particle accelerator complex. The component of the telescope is separated into two parts are,

1. A device under test (DUT) is a characterizing device. DUT is always put at a middle of the telescope.
2. The reference planes with sensors are constructed to mark a particle position when passing through DUT.

Table 3.1 Electron Beam Parameters at High-energy Beam Transport Line (HBT) (Kittimanapun et al., 2016).

listed	parameter
Particle	electron
Energy	1 GeV. 1.2 GeV.
Energy spread	-0.05%
Current	10 mA
Pulse duration	8.5 ns
Bunch length	0.5 ns
Repetition rate	0.5 Hz 0.3 Hz
Highest number of electrons per burst	10^8

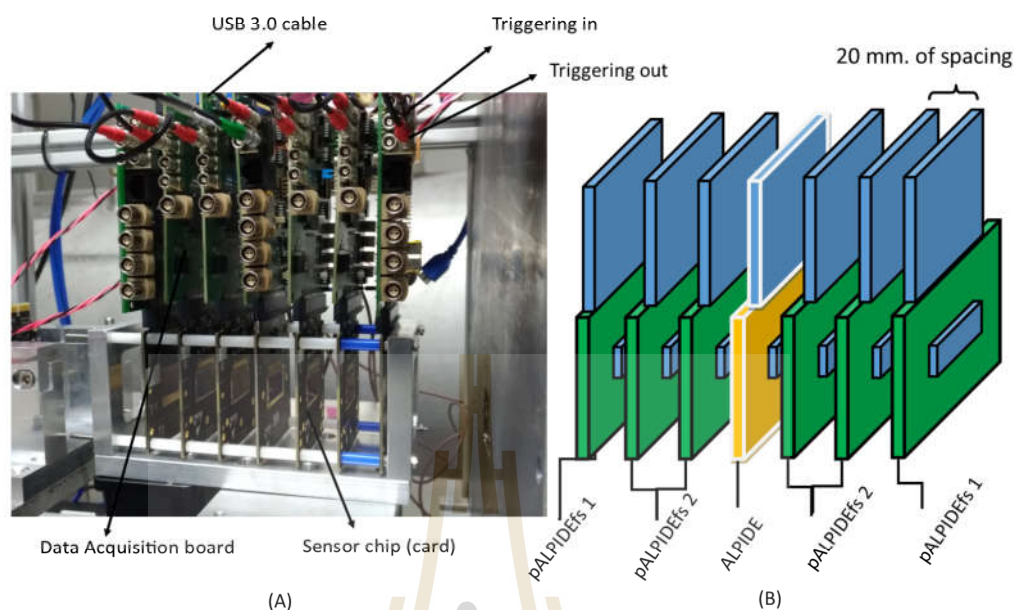


Figure 3.4 A diagram of telescope component, there are a real instrument (A) and a telescope graphic (B).

Each sensor plane needs a combination of a data acquisition board with an ALPIDE chip. Applying the main power supply by direct current power supply at 5 volts is required. The back bias voltage is applied by 0 volts for a prototype ALICE pixel detector full-scale (pALPIDEs) 1, -3 volts for pALPIDEs 2 and -3 volts of ALPIDE (as a DUT). For each of a data acquisition board is ordered by a Debug pin. A debug pin connected by the electronics jumper port followed a binary number sorting. USB 3.0 port is used to connect with a desktop for managing data. The square pulse (or triggering signal) is applied to synchronize on a data acquisition board with Synchrotron Booster. The spacing between each of ALPIDE sensor is 20 mm as shown in figure 3.4 and 3.5.

The collision information from an electron beam will be collected and ana-

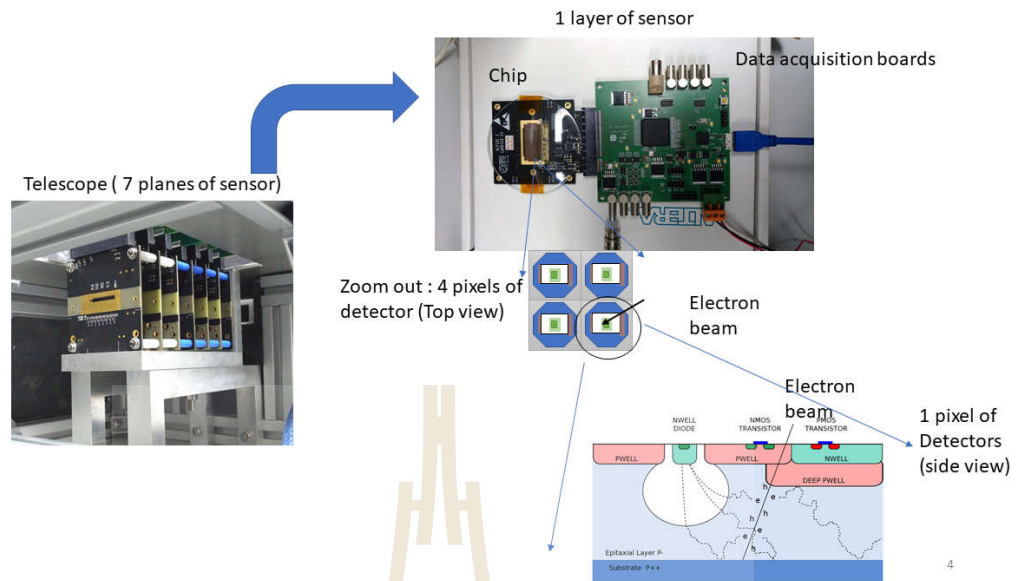


Figure 3.5 A diagram of telescope structure.

lyzed by an analysis framework. More details will be discussed in the next chapter.

CHAPTER IV

DATA TAKING AND ANALYSIS

FRAMEWORK

4.1 Test beam framework

After telescope set-up, the data needs to be collected and analyzed for sensor characterization. The EUDAQ framework is represented to collecting a data. The EUtelescope framework is used to analysis the data after data collecting.

4.1.1 Eudaq framework

Eudaq framework is a typical data acquisition framework. This framework is written based on C++ language and designed to be compatible and accessible on Linux, Mac OS X, and also Windows. The EUDAQ framework was primarily written to run the EUDET-type beam telescopes with its user-specific extensions. It has been designed, developed and used as a common DAQ having user-specific interfaces for data acquisition (Producers) and data analysis (DataConverter) (EUDAQ, 2018).

Data Taking

For EUDAQ framework start, it needs to be operated in a terminal. Four windows are the run control, the log window, the data collector and the pALPIDEfs producer as shown in figure 4.1. In the beginning, after four windows appear, the correct pALPIDEfs initial file is loaded by clicking on an "Init" white box

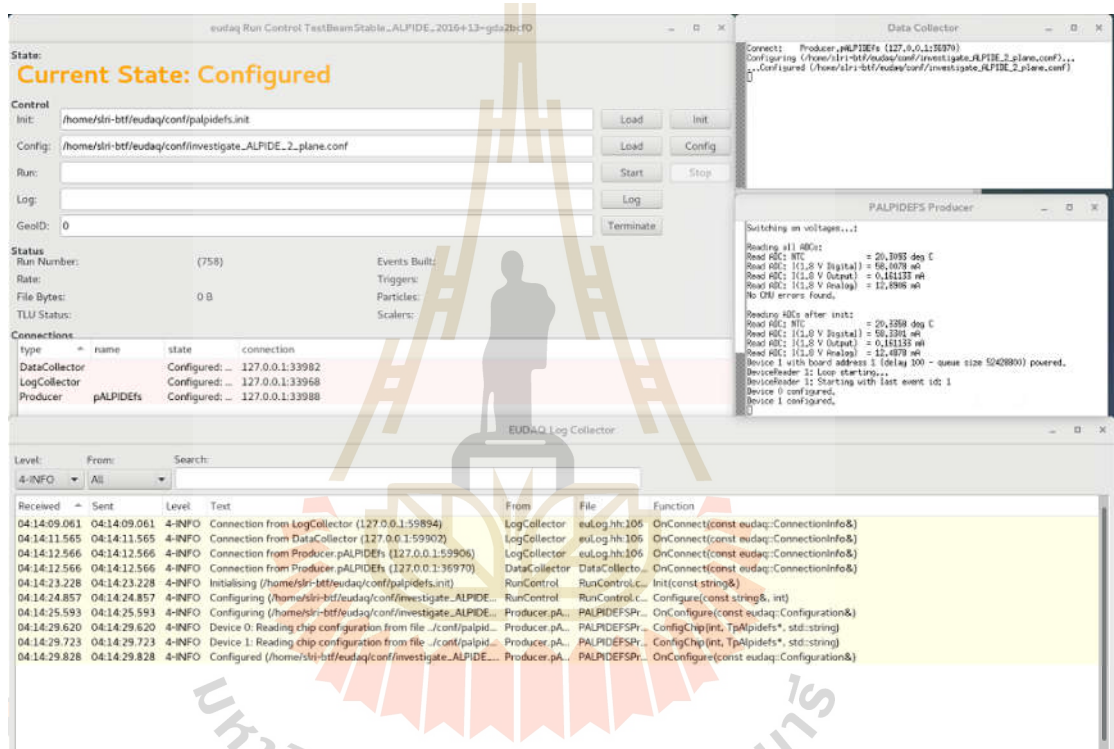


Figure 4.1 The EUDAQ framework window, there are the run control, the log window, the data collector and the pALPIDEs producers.

button. Then the run control window is permitted to configure the chips. The right pALPIDE configuration is chosen and uploaded for the telescope by clicking at "Config" box button. After this, a run can be started by clicking at "START" box button. Stop and restart a new run can be done by clicking on "STOP" box button at an EUDAQ run-control window. Any message can be declared through the log window. A status of a data can be seen at the data collector window, and the status of any chip while taking data can be observed from the pALPIDEs producer window as shown in figure 4.1.

Online Monitor

For checking recorded data in real time, the Online monitoring window can be opened by going to a binary directory and opening an online-monitoring. There are five crucial on-line monitoring windows.

- A raw hit-map for any plane in a telescope is a contour plot for the sensor detection. Contour plot or a hit marker on a diagram of seven planes sensor are shown in figure 4.2.
- A position correlation plot for position on x and y -axis of plane 0 with a nearby plane is considered for completeness support structure checking or the geometry alignment. Since all seven planes are fixed the correlation of x and y -axis of plane 0 with nearby plane should appear a solid diagonal line on every position correlation diagram as shown in figure 4.3.
- The relation of a DUT number of cluster with a hit of any number of cluster gives details of an average number of a cluster or hit at a DUT. By an average number of cluster is verified with the amount of electrons passing through a DUT as shown in figure 4.4.

- The relation of a sensor type in the telescope with an average hit is given in figure 4.5. Sensor in the telescope from most left hand side are pALPIDEfs 1, pALPIDEfs 2, pALPIDEfs 2, ALPIDEfs as DUT, pALPIDEfs 2, pALPIDEfs 2 and pALPIDEfs 1 respectively. The lowest average hits are found on the pALPIDEfs 1 because it is the first prototype without back bias voltage at 4.5 to 5 of an average hits. Higher average hits are found on the pALPIDEfs 2 since it has been improved to get a better detection efficiency than pALPIDEfs 1 by using the electronic design at 5 to 6.6 of an average hit. The highest average hits are found on ALPIDEfs since it is the final version from design and has been optimized for the best detection efficiency. Moreover, ALPIDEfs sensor can be applied a back bias voltage for depletion region producing in Silicon dies at 7.8 of an average hit.
- The relation of an event for a telescope with seven planes can be controlled by moving a tungsten wedge during the data taking. The results are shown as figure 4.6.

4.1.2 Data analysis Framework (EUTelescope)

Raw data from the EUDAQ are collected in an analysis procedure. The framework for analysis is called an EUTelescope framework. This framework is a multi-computing language. It consists of library written in several languages such as C++, Java, Python and C language. The flow chart of EUTelescope is shown in figure 4.7. The details of each step are described below.

Converter

A converter is the first procedure of an EUTelescope framework that transfers raw file from EUDAQ to Linear Collider in/output file (Korafago, 2017).

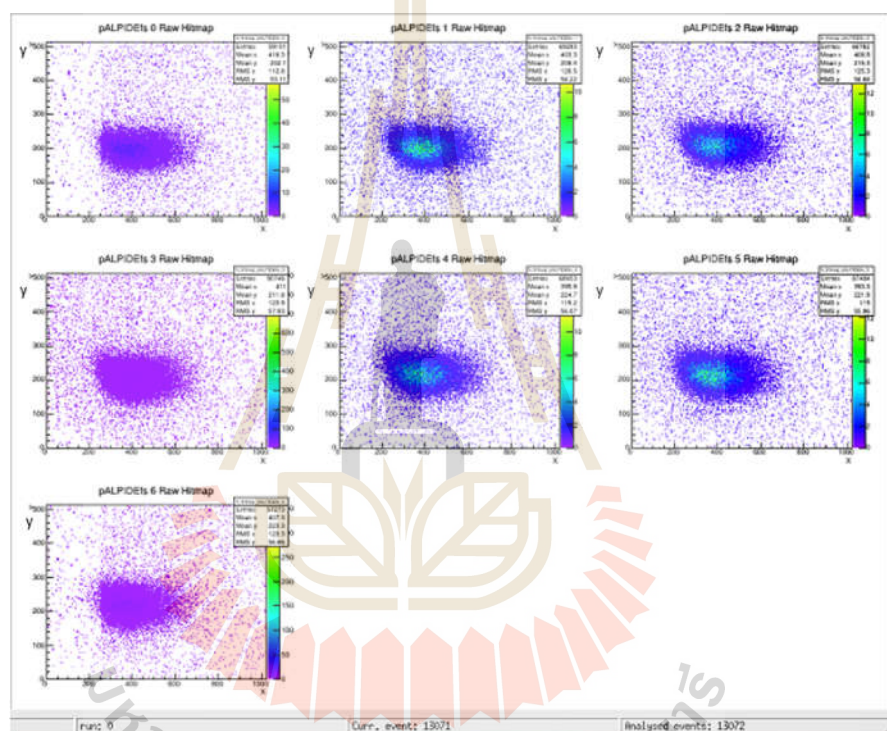


Figure 4.2 Raw hit-map for showing up an collective hit position contour plot on each sensor.

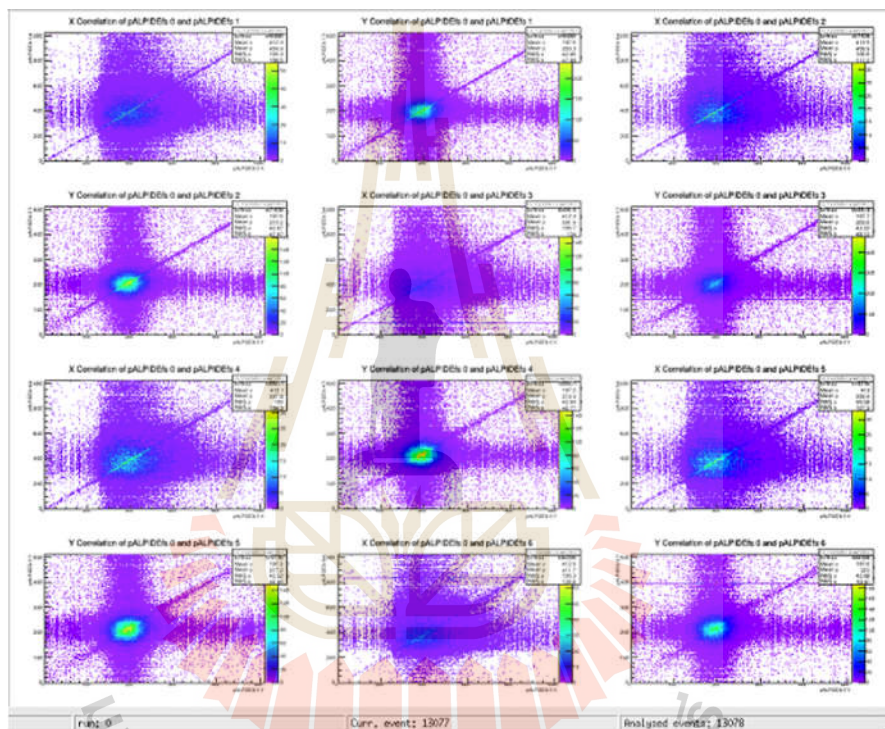


Figure 4.3 Position correlation plots for position on x and y axis of plane 0 with nearby plane(plane 1) and other couple (plane 0 with plane 2) to plane 0 with plane 6 respectively.

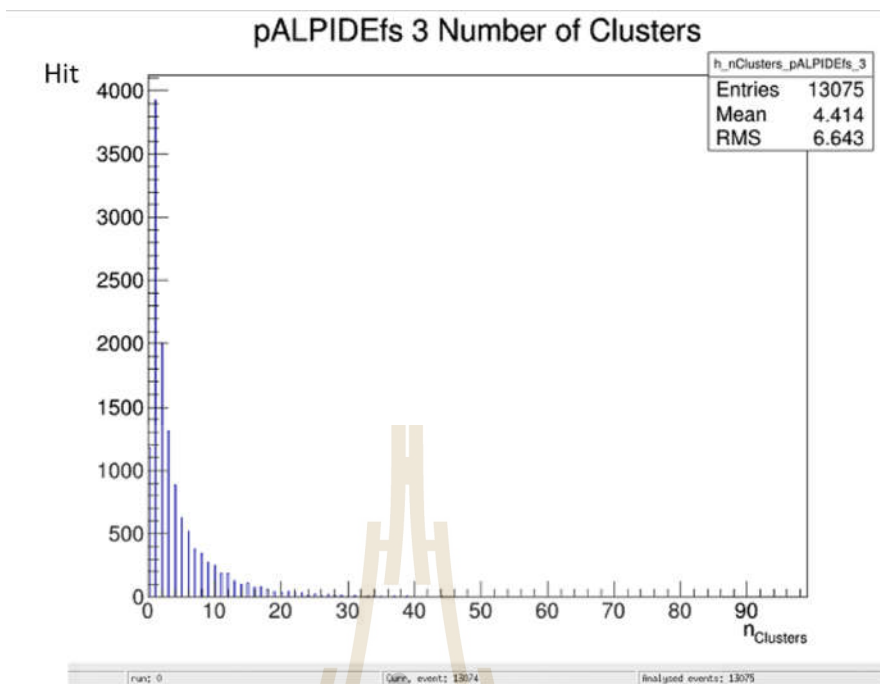


Figure 4.4 The relation of a Device Under Test (DUT) number of cluster with a hit of any number of cluster.

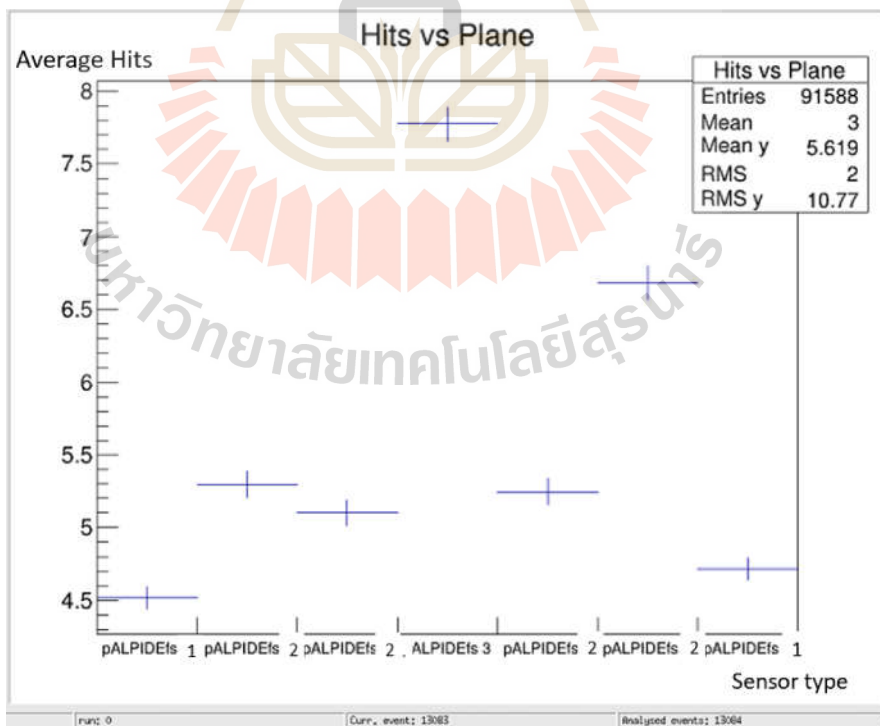


Figure 4.5 The relation of a sensor type in the telescope with an average hit of any sensor type.

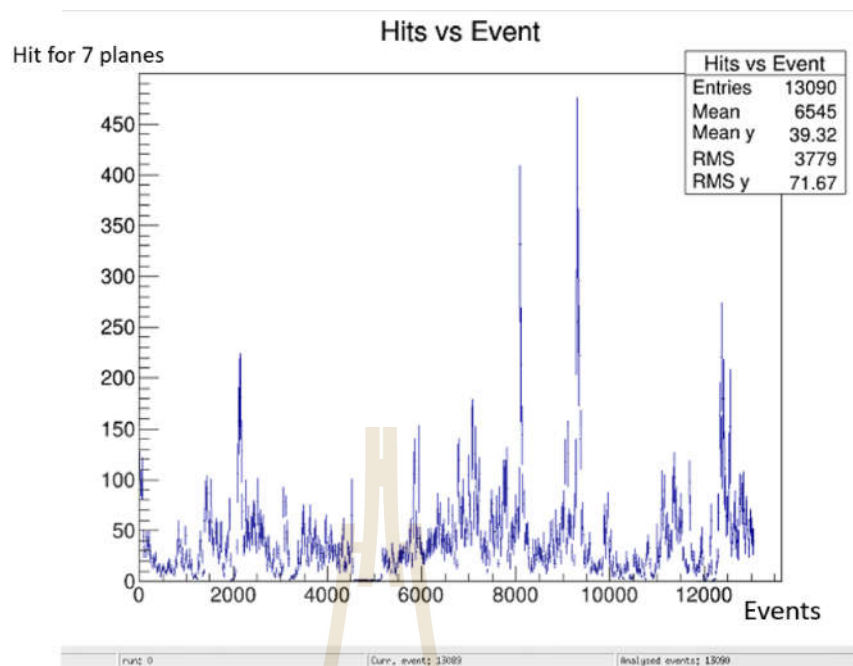


Figure 4.6 The relation of an event for a telescope with 7 plane hit of sensor.

DeadColumn

Dead Column is the second procedure of an EU telescope framework that searches for a faulty double column dead in case of a deactivated pixel. If a faulty pixel was not excluded from the analysis data, it causes reduction of a detection efficiency because a deactivated double column were not recorded while collecting a hit (Korafago, 2017).

Hotpixel

This procedure aims to find pixels which are very often firing by itself or always switch on. These pixels are called hot pixel. The hot pixel can make a problem in both alignment and fitting tracks. Searching in alignment is determined for first 10,000 events. If a pixel has a firing frequency more than a particular frequency, it is treated as a hot pixel and is cut from analysis data (Korafago, 2017).

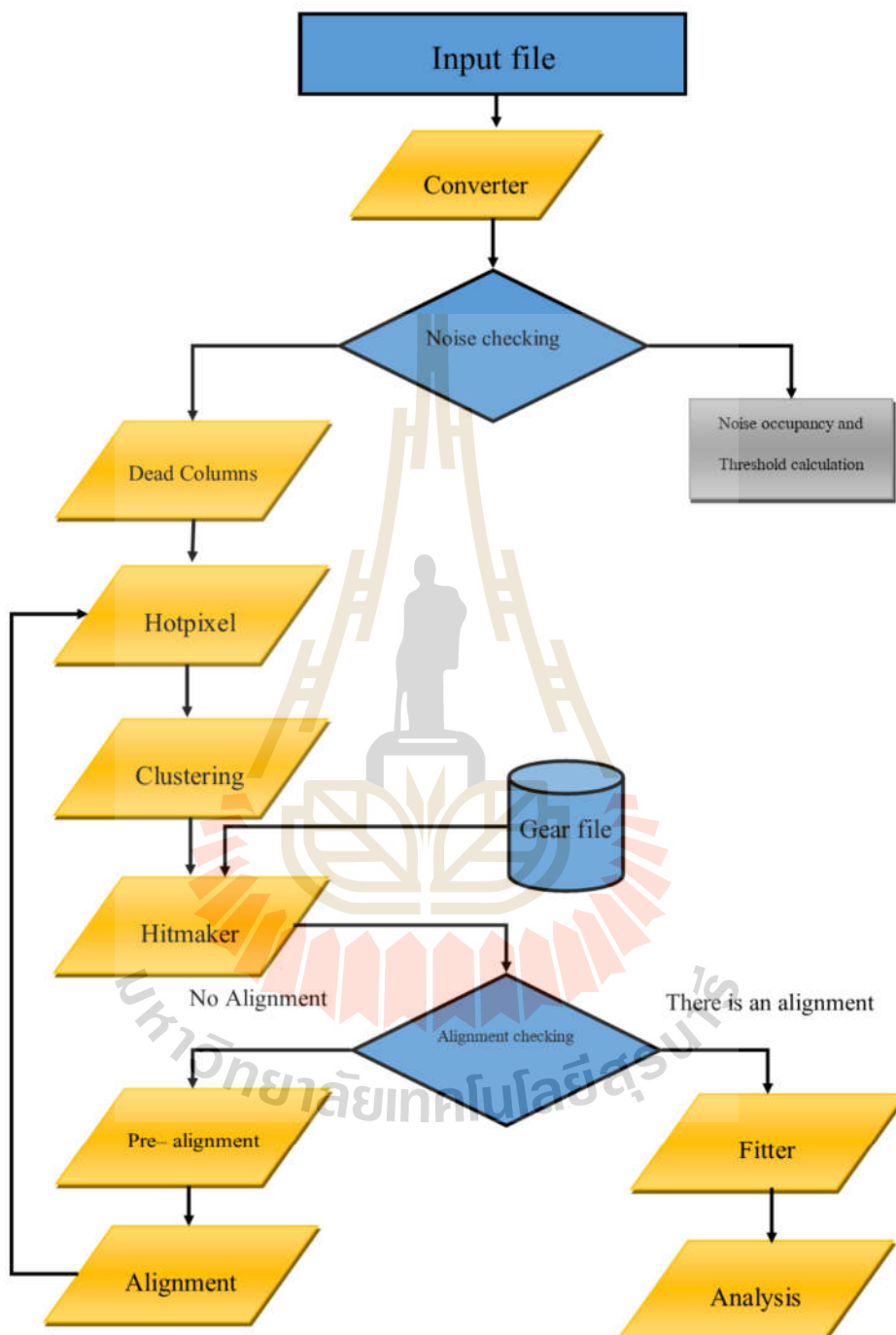


Figure 4.7 The flowchart of the EuTelescope working procedure adapted from M.korafago.

Clustering

In this procedure, pixels which are hit in the same event, are grouped in a cluster to calculate a point where data agent takes place (Korafago, 2017).

Hitmaker

After pixels are grouped to be a cluster, the center of gravity was calculated for each cluster. For this step, any cluster is represented to be a hit on its local coordinate (x,y,z) . A hit then is transferred from local coordinate to global co-ordinate under Cartesian coordinate. The middle plane is determined by an origin point $(0,0,0)$. The geometry of telescope is modified and constructed as a Geometry Application Programming Interface for Reconstruction (GEAR) file determination. Detailed of any chip configuration is set up in a GEAR file, for example, chip thickness, radiation dose, chip position and etc. The x -axis and the y -axis are planar on a horizontal direction of a global coordinate. The z -axis is along a vertical direction of a global coordinate. To correct an incompleteness of the global coordinate, an alignment needs to apply for the correctness. Due to a shift and rotation of any chips in the telescope, a position on a real global coordinate might not be the same as a position on chips (Korafago, 2017).

Pre-Alignment

To correct a missing position on a real global coordinate. An alignment is separated by two procedures: pre-alignment and alignment. In pre-alignment, a shift of any chip position on x and y coordinates are calculated for each of plane with a first plane position. It then approximates the mean distribution value from the origin position $(0,0,0)$. In this step, a calculation is included only a shift of x and y directions without considering the rotation. Furthermore, this procedure

can treat a substantial misalignment up to 3- 4 mm (Korafago, 2017).

Alignment

Alignment step is treated to find a misalignment by using a straight line tracks to fit through a hit on a chip. A χ^2 minimization can find the most proper alignment constant. In the process, a three alignment parameter for each chip is a shift of x and y coordinate and a rotation of a xy plane along the z -axis (Korafago, 2017).

Fitter

In this procedure, tracks of any plane are fitted by the track calculation. The tracking line is performed in x and y dimensions. The χ^2 minimization is used to calculate a fitting track. The fitting has two contributions: the distance from tracks to the measured hits and the scattering angle from the plane. There is a χ^2 equation for χ^2 performing (Korafago, 2017) as shown in the equation 4.1.

$$\chi^2 = \sum_{i=1}^N \left(\frac{y_i - p_i}{\sigma_i} \right)^2 \Big|_{i \neq i_{DUT}} + \sum_{i=2}^{N-1} \left(\frac{\Theta_i - \Theta_{i-1}}{\Theta_{AVG,i}} \right)^2 \Big|_{i \neq 1, N} \quad (4.1)$$

where i is an index of a plane number starting from 1, p_i is a track position on plane i , y_i is a hit position on plane i , σ_i is a resolution on plane i , $\Theta_{AVG,i}$ is an average scattering angle on plane i and θ_i is an angle of track to the normal line. For fitting, any plane can be determined to be active or passive. A hit of a passive plane is not considered for fitting, while a hit of a active plane is considered for fitting. Typically, a reference plane is treated as active but a DUT is determined as a passive plane. The mentioned parameters, in Equation 4.1. can be described as show in the figure 4.8.

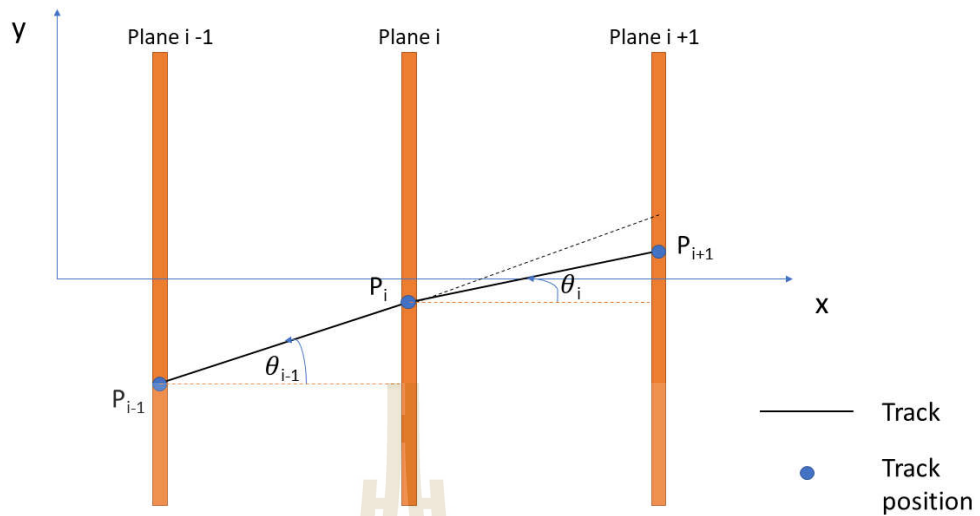


Figure 4.8 Track fitting procedure on multiple plane adapted from M.korafago.

Analysis

From the fitting procedure, the track impinging point is marked and used to calculate the position on the DUT. However, the hit on a DUT is excluded from an associated track. The associated tracks are calculated onto the analysis procedure. In practice, hits are associated with tracks even if they are closer than $100 \mu\text{m}$ in both x and y directions (Korafago, 2017). Since the beam test facility provides a 1 GeV electron beam with a speed close to the speed of light, the scattering angle on a plane is small. Finally, the detection efficiency and spatial resolution are calculated and recorded in a log file. The clusters size and the shape of a cluster are characterized. The detection efficiency can be calculated for all tracks using the equation,

$$\text{Detection efficiency} = \frac{\text{An associated tracks with hit on DUT}}{\text{All tracks on DUT}}$$

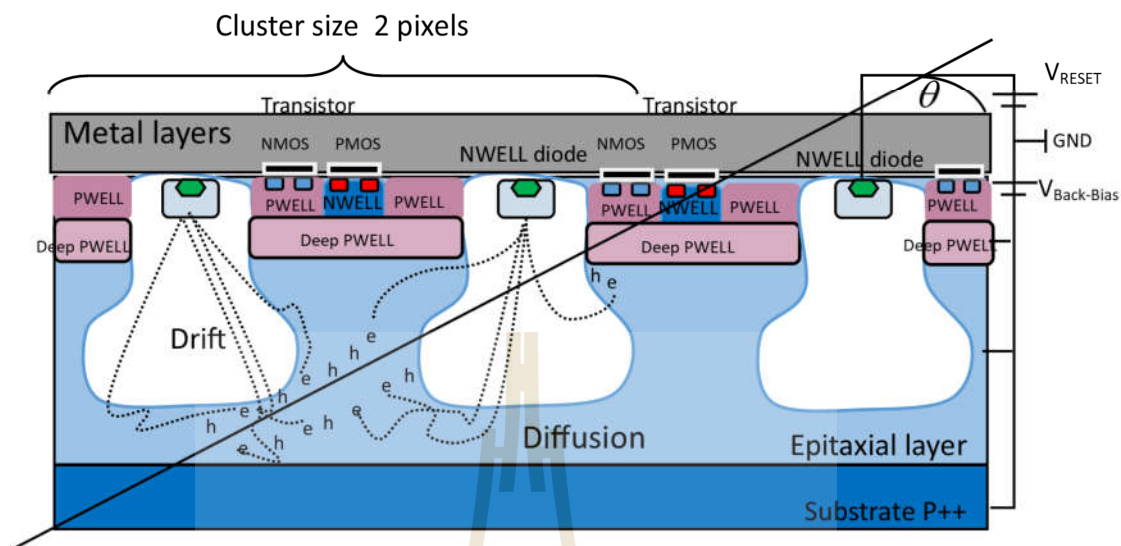


Figure 4.9 Cluster size layout that performs on a Monolithic active pixel sensor with a particle track.

Average cluster size

When the incoming charged particle passes through a silicon layer, electron-hole pairs are generated on the epitaxial layer. The induced charges from an incoming particle have generated a signal, occupied and distributed on a pixel. The average amounts of a pixel that are generated a hit signal and occupied by ionized charges called “Average cluster size.” as shown in figure 4.9.

Detection efficiency

Detection efficiency requirement of the ITS upgrade is above 99 %. The detection efficiency is calculated under a hit of a DUT. The hit was not included in the track fitting. When the hit on a DUT is interpolated with the associated track

using all planes to find where hit cross the DUT. The detection efficiency is calculated by a ratio of associated hit to all tracks and all tracks from a telescope. The detection efficiency is calculated from probability density function from Bayesian theorem (Ullrich and Xu, 2008) as shown in the following equation

$$P(\varepsilon; k; n) = \frac{(n+1)!}{k!(n-k)!} \varepsilon^k (1-\varepsilon)^{n-k} \quad (4.2)$$

where ε is a true detection efficiency which is the mode of the distribution and n is a number of event in the sample and k is a number of observed events.

Geometry Application Programming Interface for Reconstruction (GEAR) file

The GEAR file presents details that describe positions of sensors, thickness of sensors, distances between sensors, radiation length of sensors, shift distances and rotation angles of sensors with coordinates. The details are used for building the global coordinate in the Hitmaker procedure to investigate an alignment and a track fitting in an analysis procedure. In the EUTELESCOPE framework, the GEAR file is written in form of a XML file. For telescope setup, the GEAR file is needed to be modified to match the telescope setup.

After an analysis strategy, all results that will be demonstrated and discussed in the next chapter.

CHAPTER V

RESULT AND DISCUSSION

5.1 Test beam commission

To see whether the test beam commissioning process is successfully or not, we have to look at the preliminary results of the telescope setting. The raw hit map is the first result which shows a real hit on the telescope. For each of hit map, there is the highest distribution at a center of a cluster (darkest area) and lower distribution at surrounding. The telescope consists of pALPIDEs 1 in plane 0 and 6, pALPIDEs 2 in plane 1,2, 4 and 5 , ALPIDE (as DUT) in plane 3. Figure 5.1 shows the hit maps of all planes. Next, the correlation position contour plots are shown to investigate an arrangement of the telescope. A relation of an hit position with a x -axis hit position of nearby plane is investigated to verify if there is any imperfections in the telescope structure. The perfect arrangements in each plane of the telescope is performed by a solid diagonal line of a correlation position plot. From correlation plot results, the solid diagonal lines of a correlation position plot for x and y axes are presented as shown in figure 5.2 and 5.3.

5.2 Test beam data analysis

Not all raw data, can be used for analysis and obtained a detection efficiency. There were 19 sets of suitable data or “good run” as shown in table 5.1 that can be used without modification. There could also be some data that were not able to pass the analysis procedure due to limits of data analysis condition. In

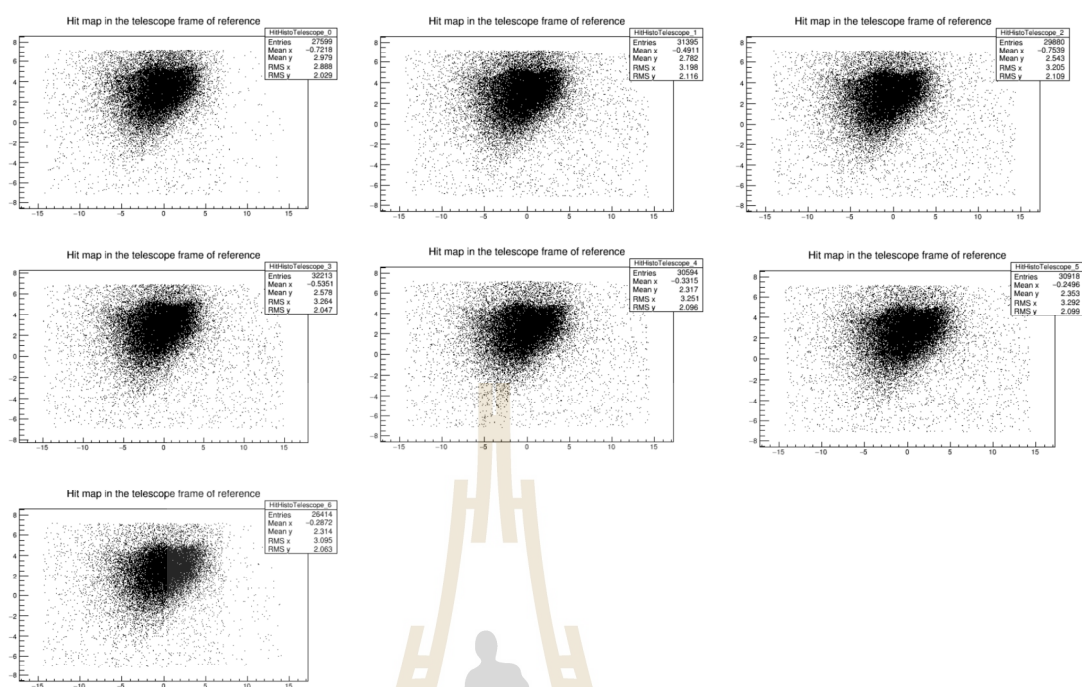


Figure 5.1 Hitmap from reference frames of a telescope.

table 5.2, we present 18 sets of data that receive the error when we performed the analysis. However, with some modifications, we still can extract useful information as needed. In next section, we mention how to handle such analysis errors.

5.2.1 Beam data modification in case of a problem

In case of analysis problem, we can classify the problems into three main categories.

1. There is an error at dead column due to the maximum average hit array for any plane over 100 hits.
2. There is a problem of hot pixel due to a high-intensity beam. There exists a very high firing frequency much more than a particular frequency.

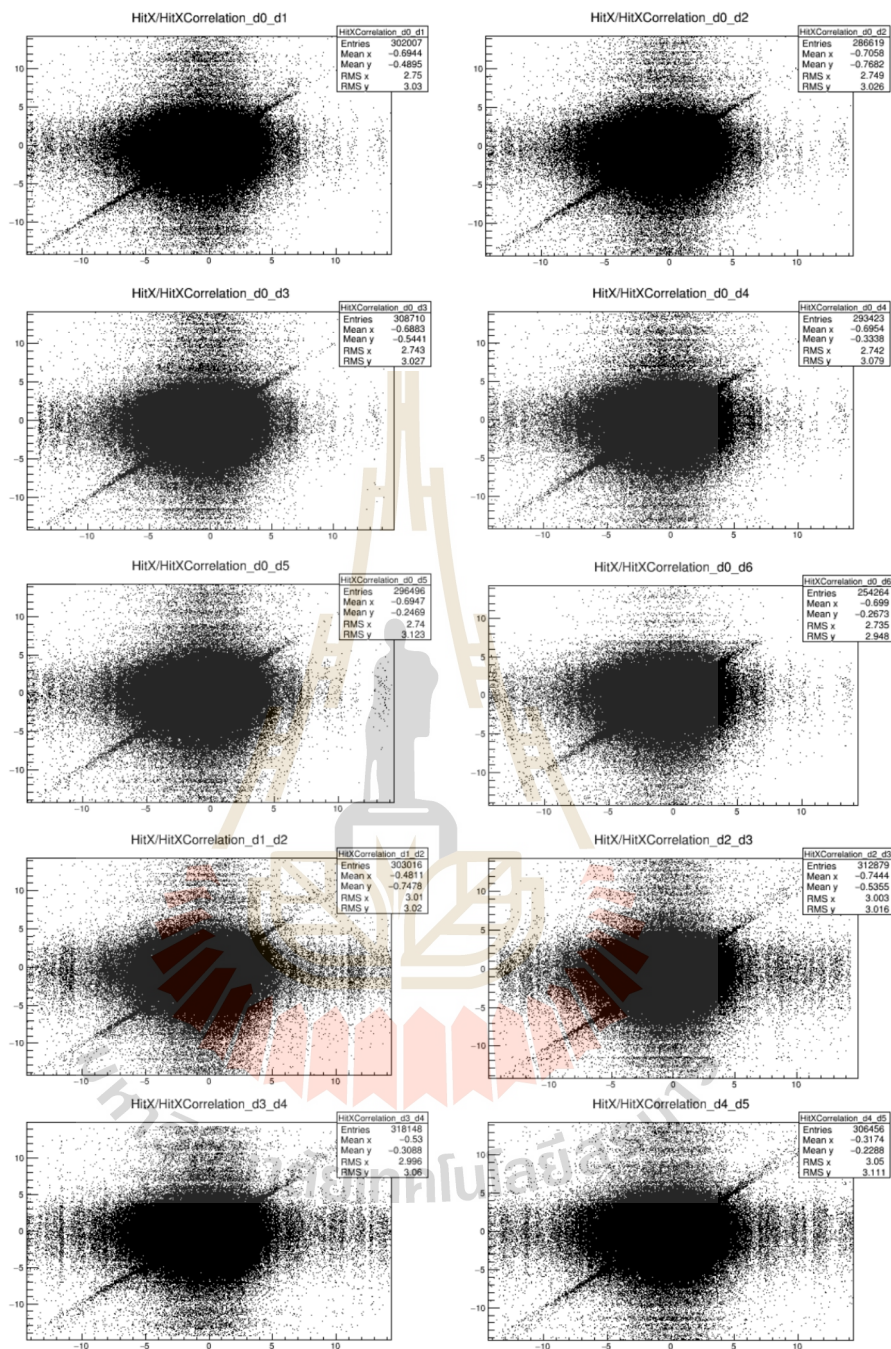


Figure 5.2 Correlation plots of x axis on plane 0 with plane 1, 2, 3, 4, 5 and 6; plane 1 with plane 2; plane 2 with plane 3; plane 3 with plane 4; and plane 4 with plane 5, respectively. (ordering from left to right and top to bottom) from a reference frame of a telescope.

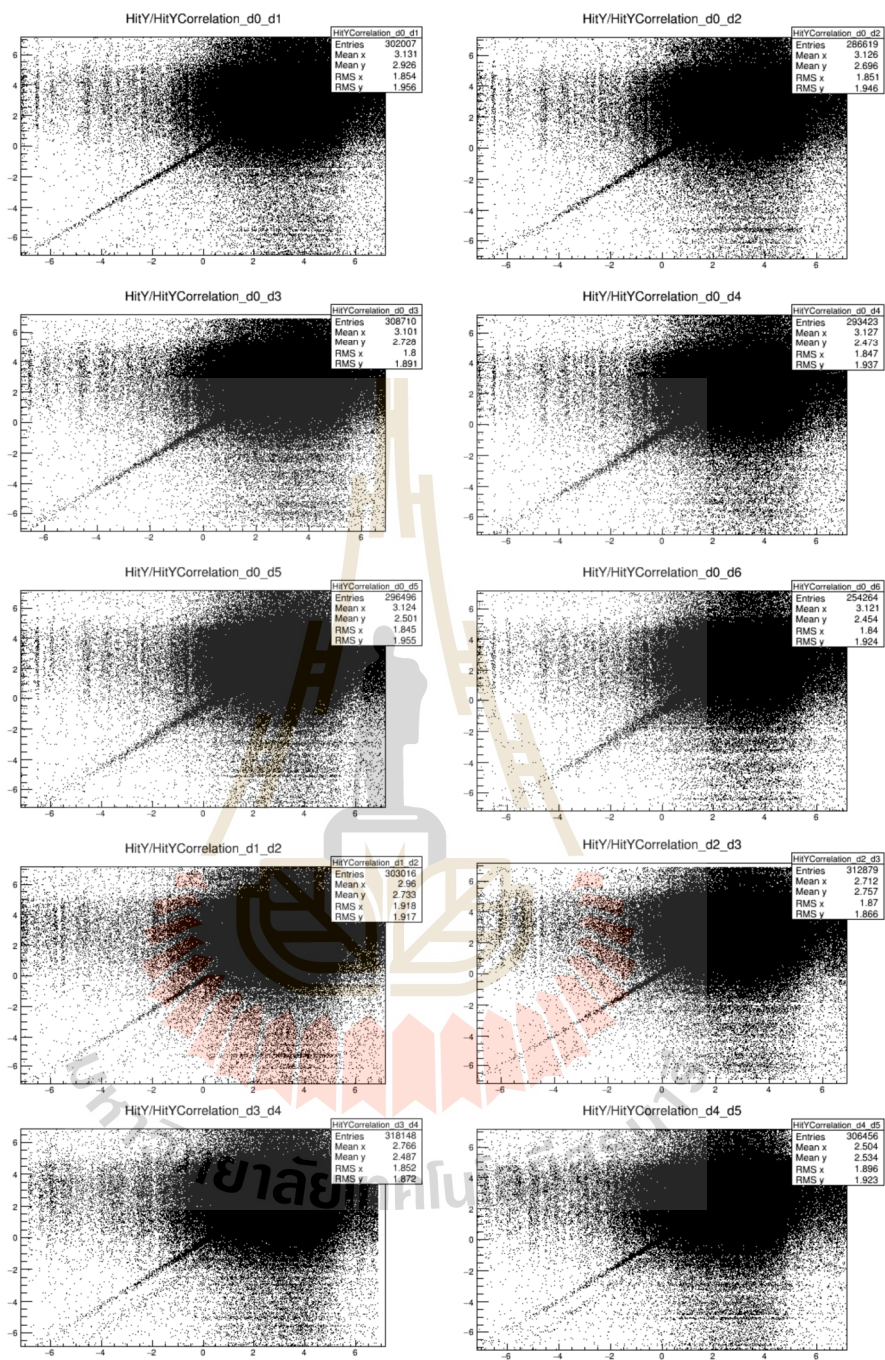


Figure 5.3 Correlation plots of y axis on plane 0 with plane 1, 2, 3, 4, 5 and 6; plane 1 with plane 2, plane 2 with plane 3; plane 3 with plane 4; and plane 4 with plane 5, respectively.(ordering from left to right and top to bottom) from a reference frame of a telescope.

3. An alignment procedure fails due to a high-intensity beam that causes a divergent trajectory of a beam.

5.2.2 Modification

To modify any error in a analysis process, The analysis parameters are needed to be modified for proper analysis conditions,

1. An error at dead column can be solved by extending a maximum average hit array for any plane over 100 hit arrays to 200 hit arrays.
2. The problem from hot pixel is solved by increasing a maximum allow firing frequency from 0.0001 (0.01%) of number event of hot pixel (default setting as 9999 events) to 0.001 (0.1%) of number event of hot pixel. In case of the high intensity, a high frequent hit on a pixel in the same event is considered to be a hot pixel because a firing rate is more than a maximum allows firing frequency. With this reason, the problem can be solved by increasing a maximum allow firing frequency.
3. An alignment procedure also can be failed due to a divergent trajectory of a beam in a high-intensity beam. The alignment problem can be solved by setting a common alignment from the complete alignment data. The perfect alignment XML file is used instead of its alignment file.

To take run data from electron beam, an electron beam is ejected to characterize the ALPIDE sensor at Beam Test Facility station.

5.3 Relation of high intensity beam

After some modifications, we have 37 sets of data that can pass the analysis procedure. All datas can be used to calculate the detection efficiency and the

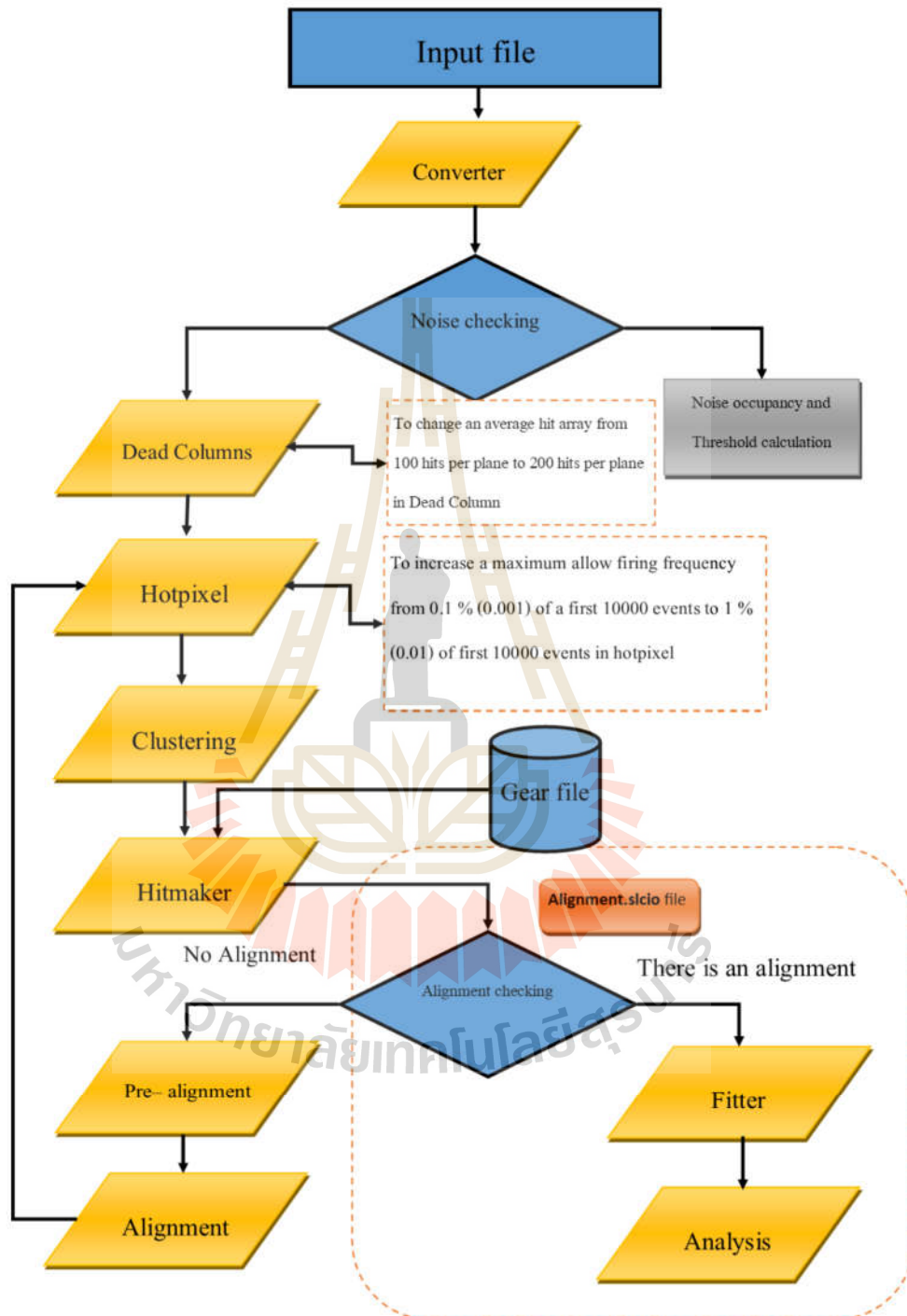


Figure 5.4 Flowchart of an Eutelescope working procedure adapted from M.korafago.

Table 5.1 Results for good run before analysis modification.

number	run number	Repetition rate (Hertz)	Taking data time (hrs.)	Energy (GeV.)	Detection efficiency
1	73	0.5	7	1.0	0.9449
2	174	0.5	7	1.0	0.9989
3	188	0.5	7	1.0	0.9991
4	190	0.5	7	1.0	1
5	193	0.5	7	1.0	0.9982
6	194	0.5	7	1.0	0.9985
7	199	0.5	7	1.0	0.9997
8	219	0.5	7	1.0	0.9846
9	225	0.5	7	1.0	0.9613
10	227	0.5	7	1.0	0.9553
11	252	0.5	7	1.0	0.9886
12	298	0.5	7	1.0	0.999
13	320	0.5	7	1.0	0.9989
14	337	0.5	7	1.0	0.9987
15	343	0.5	7	1.0	0.9986
16	350	0.5	7	1.0	0.9993
17	352	0.5	7	1.0	0.9986
18	434	0.5	7	1.0	0.9992
19	441	0.5	7	1.0	0.9973

Table 5.2 List of run data in case of problem during analysis.

Number	Run number	Error message (error procedure in Eutelescope)
1	95	Too few tracks found in DUT run 95(Hotpixel)
2	206	More than 2 noise planes (planes 0 1 2 3 4 5 6) in run 206(DeadColumns)
3	242	Too few tracks found in DUT run 242(Hotpixel)
4	289	Too few tracks found in DUT run 289(Hotpixel)
5	312	Too few tracks found in DUT run 312(Hotpixel)
6	317	Too few tracks found in DUT run 317(Hotpixel)
7	338	Too few tracks found in DUT run 338(Hotpixel)
8	348	Too few tracks found in DUT run 348(Hotpixel)
9	356	More than 2 noise planes (planes 0 1 2 3 4 5 6) in run 356 (DeadColumns)
10	358	More than 2 noise planes (planes 1 2 3 4 5) in run 358 (DeadColumns)
11	359	Too few tracks found in DUT run 359 (Hotpixel)
12	361	More than 2 noise planes (planes 1 2 3 4 5) in run 361(DeadColumns)
13	367	More than 2 noise planes (planes 1 2 3 4 5) in run 367(DeadColumns)
14	417	More than 2-noise planes (planes 1 2 3 4 5) in run 417(DeadColumns)
15	444	Too few tracks found in DUT run 444 (Hotpixel)
16	489	Too few tracks found in DUT run 489 (Hotpixel)
17	491	Alignment step failed, output is strange in run 491(Alignment)
18	494	Alignment step failed, output is strange in run 494(Alignment)

cluster size. In this research, the numbers of cluster of DUT is interested and used to study the effect of an ALPIDE characterization. The number of cluster of DUT starts from 3.82 to 45.27. This study focuses on the relation of the number of cluster of DUT and the cluster size together with a DUT detection efficiency. We find that the average cluster-size is 1.98 number of pixels as shown in figure 5.5. From a cluster size, a variation of number cluster does not have any effect on the ALPIDE cluster-size. Furthermore, we have plotted the relation between the number of cluster of DUT and the DUT detection efficiency. Our calculate detection efficiency is in agreement with the ITS upgrade requirements which is 99 %. The increase of the number of cluster of DUT does not have an effect on an ALPIDE detection efficiency shown in figure 5.6.

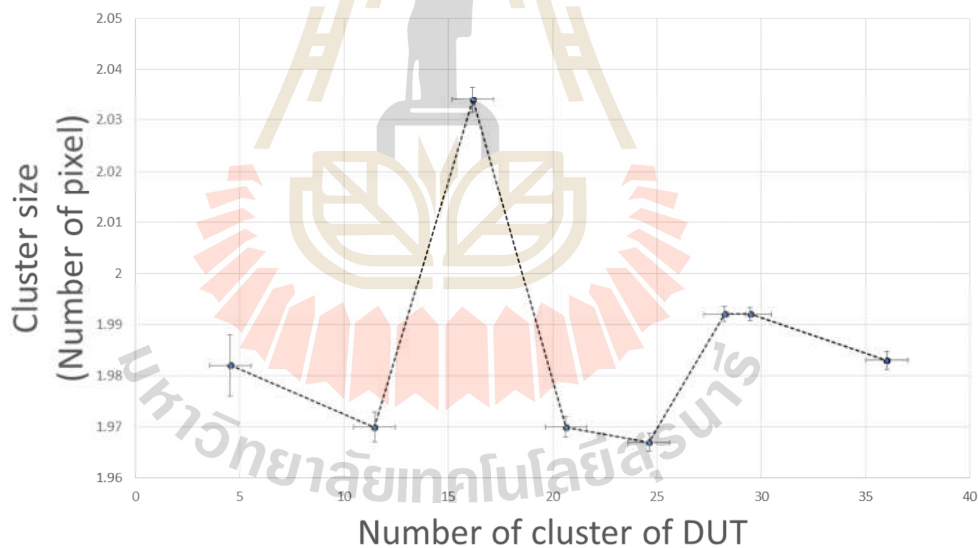


Figure 5.5 Relation of the cluster size of an ALPIDE chip (unit in a number of pixel) with the number of cluster of DUT.

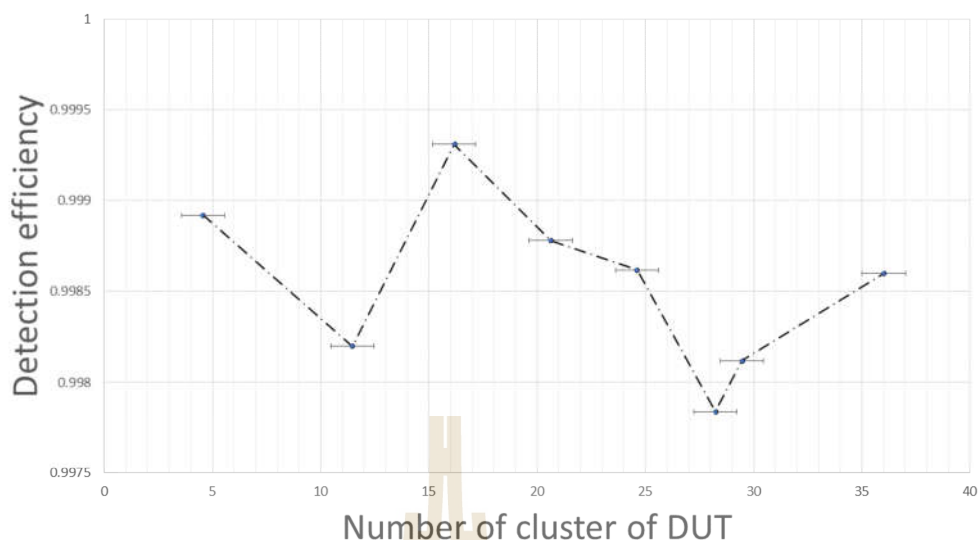


Figure 5.6 Relation of Detection efficiency with a number of cluster of DUT.

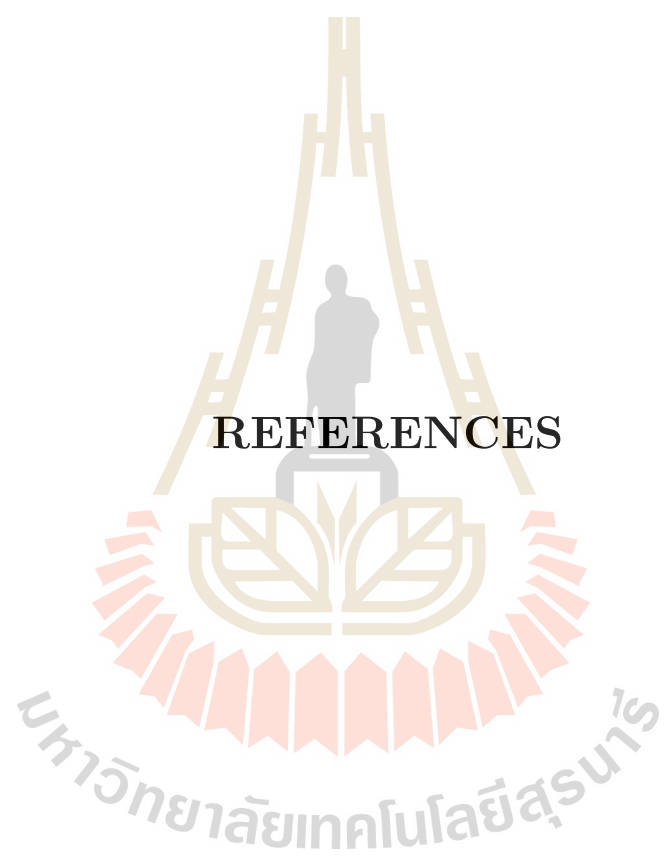
5.4 Discussion

We compare our results with the results using the test beam of the 180 GeV/c pion at the CERN SPS accelerator. Their results show a detection efficiency of pALPIDEfs 2 as a function of threshold current (varying from 200 to 1000 pAmp) at -3 volts of a back-bias voltage and the detection efficiency is over 99%. The cluster size is constant at two pixels (Reidt, 2016).

CHAPTER VI

CONCLUSION

From our the results, the 1 GeV electron beam test-beam commission has demonstrated a success telescope setup for ALICE pixel detector(ALPIDE) sensor characterization. The raw hit map and position correlation have been performed and shown the electron beam on a telescope. In the analysis procedure, some data can be adequately characterized to provide sensor detection efficiency. While, there are some data failed to pass an analysis procedure due to the dead-Column finder, hot pixel finder, and alignment. The problems can be solved by adjusting parameters of the analysis configuration. The number of a cluster on the DUT does not effect the cluster size and detection efficiency of the ALPIDE. In our work, the average cluster size of the ALPIDE sensor is 1.98 pixel and the ALPIDE sensor detection efficiency is over 99 % which agree with ALICE ITS upgraded requirements . Further, the future work is possible to characterize an ALPIDE sensor with an inclined angle condition of the DUT at a different bunch intensity of electron beam.



REFERENCES

REFERENCES

- Aamodt, K., Abrahantes Quintana, A., Achenbach, R., Acounis, S., Adamová, D., Adler, C., Aggarwal, M., Agnese, F., Aglieri Rinella, G., Ahammed, Z., Ahmad, A., Ahmad, N., Ahmad, S., Akindinov, A., Akishin, P., and other (2008). The ALICE experiment at the CERN LHC. **Journal of Instrumentation**, 3(08):S08002–S08002.
- Abelev, B., Adam, J., Adamov´a, D., Aggarwa, M., Aglieri Rinella, G., Agnello, M., Agostinelli, A., Agrawa, N., Ahammed, Z., Ahmad, N., Ahmad Masoodi, A., Ahmed, I., Ahn, S., Ahn, S., Aimo, I., and others (2014). Technical design report for the upgrade of the alice inner tracking system. **Journal of Physics G: Nuclear and Particle Physics**, 41(8):087002.
- acceleratorSLRI (2018a). Booster synchrotron (syn). <http://accelerator.slri.or.th/parameters/syn>.
- acceleratorSLRI (2018b). High energy beam transport line (hbt). <http://accelerator.slri.or.th/parameters/hbt>.
- Aglieri, G., Cavicchioli, C., Chalmet, P. L., Chanlek, N., Collu, A., Giubilato, P., Hillemanns, H., Junique, A., Keil, M., Kim, D., and other (2013). Monolithic active pixel sensor development for the upgrade of the ALICE inner tracking system. **Journal of Instrumentation**, 8(12):C12041–C12041.

- ALICE ITS upgrade collaboration (2016). Alpile operations manual. **WP5 ITS upgrade group database**, 1(0.3).
- ALICEwebsite (2019). The alice experiment, overview of a particle detector. <http://aliceinfo.cern.ch/Public/en/Chapter2/Chap2InsideAlice-en.html>. Accessed: 2019-02-11.
- Beringer, J., Arguin, J. F., Barnett, R. M., Copic, K., Dahl, O., Groom, D. E., Lin, C. J., Lys, J., Murayama, H., Wohl, C. G., Yao, W. M., Zyla, P. A., Amsler, C., Antonelli, M., Asner, D. M., and others (2012). Review of particle physics. **Phys. Rev. D**, 86:010001.
- EUDAQ, D. (2018). Eudaq framework. <https://telescopes.desy.de/EUDAQ#Manual>.
- Grosse-Oetringhaus, J. (2014). Eudaq for palpidefs - installation and usage manual. **CERN ALICE ITS upgrade technical note**. first revised Aug 24, 2014.
- Keil, M. (2017). Alpile software - user manual. **WP5 ITS upgrade group database**, 1.
- Kittimanapun, K., Chanlek, N., Juntong, N., Cheedket, S., Klysubun, P., Krainara, S., Sittisard, K., and Supajeerapan, S. (2016). Slri beam test facility development project. **Proceedings of IPAC**. ISBN 978-3-95450-147-2, BUSAN, Korea.
- Korafago, M. (2017). Summary of the test beam results of the palpide-1. **ALICE-INT-2017-001, ALICE CERN technique report**.
- Kushpil, S. (2016). Upgrade of the alice inner tracking system. **Journal of Physics: Conference Series** 675.

Leo, W. R. (1993). *Techniques for Nuclear and Particle Physics Experiments*. Springer-Verlag Berlin Heidelberg GmbH.

Mager, M. (2016). Alpide, the monolithic active pixel sensor for the alice its upgrade. **Nuclear Instruments and Methods in Physics Research Section A** Accelerators, Spectrometers, Detectors and Associated Equipment, 824: 434 – 438.

Meroli, S. (2013). Multiple coulomb scattering, in-depth study of phenomena characterizing the passage of ionizing particles through semiconductor layers. **CERN database git** available at www.cern.ch/meroli or Stefano.Meroli@gmail.com.

Reidt, F. (2016). *Studies for the ALICE Inner Tracking System Upgrade*. PhD thesis, **European Organization for Nuclear Research (CERN) and Physikalisches Institut, University of Heidelberg**.

SLRI (2018). What is synchrotron light. <https://www.slri.or.th/en/what-is-synchrotron-light.html>.

SLRIlayout (2018). Machine layout. <https://www.slri.or.th/en/machine/machine-layout.html>.

SLRILINAC (2018). Linac structure layout. <https://www.slri.or.th/en/machine/linac.html>.

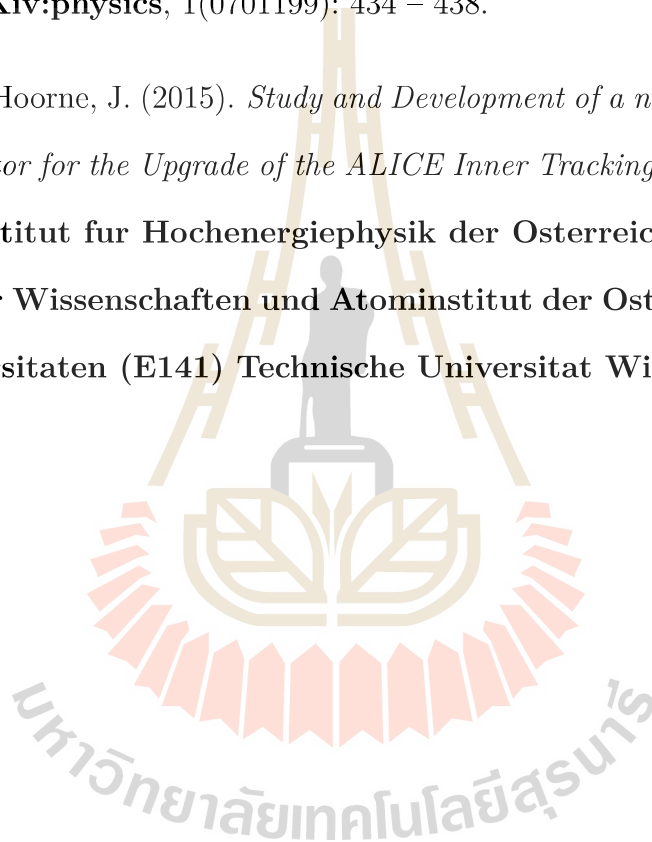
Snoeys, W. (2014). Cmos monolithic active pixel sensors for high energy physics. **Nuclear Instruments and Methods in Physics Research Section A: Accelerators, Spectrometers, Detectors and Associated Equipment**, 765:167 – 171. HSTD-9 2013 - Proceedings of the 9th In-

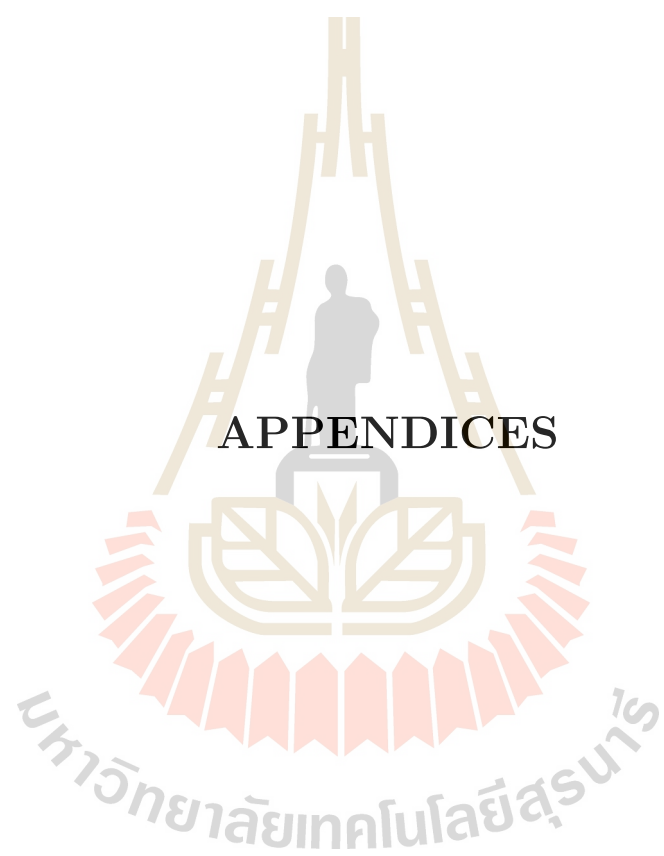
ternational at Hiroshima Symposium on Development and Application of Semiconductor Tracking Detectors.

Tsai, Y.-S. (1974). Pair production and bremsstrahlung of charged leptons. **Rev. Mod. Phys.**, 46:815–851.

Ullrich, T. and Xu, Z. (2008). Treatment of errors in efficiency calculations. **arXiv:physics**, 1(0701199): 434 – 438.

Willem van Hoorne, J. (2015). *Study and Development of a novel Silicon Pixel Detector for the Upgrade of the ALICE Inner Tracking System*. PhD thesis, **Institut für Hochenergiephysik der Österreichischen Akademie der Wissenschaften und Atominstitut der Österreichischen Universitäten (E141) Technische Universität Wien**.





APPENDIX A

SLRI ACCELERATOR

A Synchrotron Light Research Institute (SLRI) provides a service task to produce an electromagnetic wave (SLRI, 2018). There are four main components to produce an electron bunch.

- A gun filament in an electron gun is heated by electricity current and then electron from metal is released by a thermionic process (energy is above an electron work function). After this, an electron is pulled to linear accelerator by an electric field (Fig A.1).
- Linear Accelerator is an accelerator that accelerates an electron on a straight direction. There are two sections of Linear Accelerators shown in figure A.2. For each Linear Accelerator, there are
 - Accelerator tube length is 2.3 m
 - 60 cavities of copper disks
 - Accelerator type : constant impedance traveling wave Linear Accelerator (LINAC)
 - Electron Energy Output = 24 MeV (for first LINAC) and 40 MeV (for second LINAC)
 - Phase advance is $2\pi/3$ (SLRILINAC, 2018)
- Synchrotron Booster is a circular accelerator which boosts up the energy of electron from 40 MeV to 1 GeV. It is a 43.19 m of a circumference. To

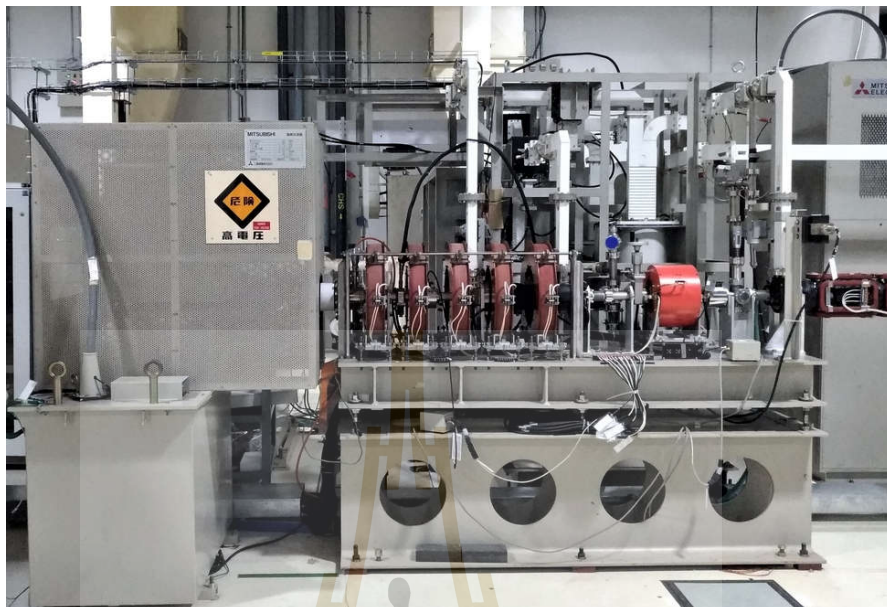


Figure A.1 An Electron gun at Synchrotron Light Research Institute.



Figure A.2 A Linear Accelerator (LINAC) at Synchrotron Light Research Institute.



Figure A.3 Synchrotron booster at Synchrotron Light Research Institute.

electron energy ramping up, an electron current about 30 mA is filled in the synchrotron Booster at repetition rate 0.5 Hz. The radio frequency at 118.000 MHz is applied to accelerate an electron in cavity for maximum RF voltage of 60 kV under the chamber pressure (with beam) less than 1×10^{-6} torr (SLRI layout, 2018) (accelerator SLRI, 2018a) as shown in figure A.3. Details of a magnet in Synchrotron Booster are

- Bending magnet, There are 12 magnets
- Quadrupole magnet, There are 12 pieces of focusing quadrupole magnets and 6 pieces of de-focusing quadrupole magnets with the following properties are
 1. Mechanical core length is 0.25 m.
 2. Maximum current (for focusing quadrupole) is 585 A.
 3. Maximum current (for de-focusing quadrupole) is 435 A.
- Steering magnet, There are 6 pieces of magnets. It can be separated as
 - * Vertical steering magnet, with 12 A of a maximum current.

- * Vertical steering magnet, with 12 A of a maximum current.
- Bump magnet,
 - * Maximum current is 60 - 370 A.
 - * Pulse width is 12 μ sec.
- Injection Septum magnet (Y-SEM1)
- Extraction Septum Magnet (Y-SMD)
- Kicker magnet (Y-KM)
- High-energy Beam Transport (HBT) is a connecting point to the transport 1 GeV electron beam from Synchrotron Booster to Storage ring. HBT is a transport point consisting of many magnets to adjust an electron beam profile before sending to the beam test facility at the end of an underground station. Components of magnets at HBT are shown (acceleratorSLRI, 2018b) in figure A.4.
 - Total length is 45.94 m.
 - Beam Energy is 1.0 GeV.
 - Magnet Parameters
 - * H-BH1 (Bending horizontal magnet 1)
 - * H-BH2 (Bending horizontal magnet 2)
 - * H-BV1(Bending vertical magnet 1) and H-BV2 (Bending vertical magnet 2)
 - * Quadrupole magnets (8 quadrupole magnets).
 1. Quadrupole defocus magnets 1 (QD 1)
 2. Quadrupole focus magnets 2 (QF 2)



Figure A.4 High-energy Beam Transport at Synchrotron Light Research Institute.

3. Quadrupole defocus magnets 3 (QD 3)
 4. Quadrupole focus magnets 4 (QF 4)
 5. Quadrupole focus magnets 5 (QF 5)
 6. Quadrupole defocus magnets 6 (QD 6)
 7. Quadrupole focus magnets 7 (QF 7)
 8. Quadrupole defocus magnets 8 (QD 8)
- * Steering magnet,
- Steering Horizontal magnet(2 magnets) (STH)
 - Steering vertical magnet(5 magnets) (STV)

Magnetic setting for Beam Test Facility station

A magnet set is defined to produce an electron beam for the Beam Test Facility station. There are two stations Synchrotron booster magnet and High-energy Beam Transport line. For any station, the strength of the magnetic field can be determined by a magnet power supply. Synchrotron booster magnet are

Table A.1 Settings of Synchrotron booster magnet power supply.

Symbol	Magnet	voltage
	Description	(Volts)
Y-BM-M	B magnet PS	none
Y-QF-M	QF magnet PS	none
Y-QD-M	QD magnet PS	none
Y-KM-M	Kicker magnet PS	50
Y-SMI-M	In-Septrum magnet PS	181.5
Y-SMD-M	Ex-Septrum magnet PS	500.0
Y-BMP-M1	Bump magnet PS1	503.0
Y-BMP-M2	Bump magnet PS2	503.0
Y-BMP-M3	Bump magnet PS3	498.0
Y-BMP-M4	Bump magnet PS4	498.0

shown in Table A.1. For the beam profile shape, High-energy Beam Transport line magnets are used to adjust the form of an electron beam for Beam Test Facility station. For the electron beam profile, there are two types. First, a point beam profile is often used to collect data. Some examples are shown in figure A.5. Parameters for the High-energy beam transport line (HBT) magnet are given in Table A.2. Second, a full beam profile is used to study an ALPIDE performance for all sensor areas as shown in figure A.6. The High-energy beam transport line magnet set up parameters in this case are shown as table A.3. If a quadrupole defocusing current is increased, a beam profile radius will be increased. A steering magnet can be used for a beam position adjustment. A horizontal steering magnet is used to adjusting a beam position on the x-axis of a telescope. Also, a vertical steering magnet is used to change a beam position on the y-axis of a telescope.

Table A.2 Settings of High-energy Beam Transport(HBT) line magnet power supply for a point beam profile.

Symbol	Instruments	Current
	Description	(Amp.)
H-BV-M1	Bending vertical magnet power supply 1	0.0
H-BH-M1	Bending horizontal magnet power supply 1	84.39
H-BV-M2	Bending vertical magnet power supply 2	0.0
H-BH-M2	Bending horizontal magnet power supply 2	0.0
H-QD-M1	Quadrupole de-focus magnet power supply 1	15.0
H-QF-M2	Quadrupole focus magnet power supply 2	18.0
H-QD-M3	Quadrupole de-focus magnet power supply 3	11.2
H-QF-M4	Quadrupole focus magnet power supply 4	12.5
H-QF-M5	Quadrupole focus magnet power supply 5	0.0
H-QD-M6	Quadrupole de-focus magnet power supply 6	0.0
H-QF-M7	Quadrupole focus magnet power supply 7	0.0
H-QD-M8	Quadrupole de-focus magnet power supply 8	0.0
H-STV-M1	Steering vertical magnet power supply 1	14.0
H-STV-M2	Steering vertical magnet power supply 2	-11.0
H-STH-M3	Steering horizontal magnet power supply 3	-7.7
H-STV-M4	Steering vertical magnet power supply 4	1.3
H-STH-M5	Steering horizontal magnet power supply 5	0.0
H-STH-M6	Steering horizontal magnet power supply 6	0.0
H-STV-M7	Steering vertical magnet power supply 7	0.0

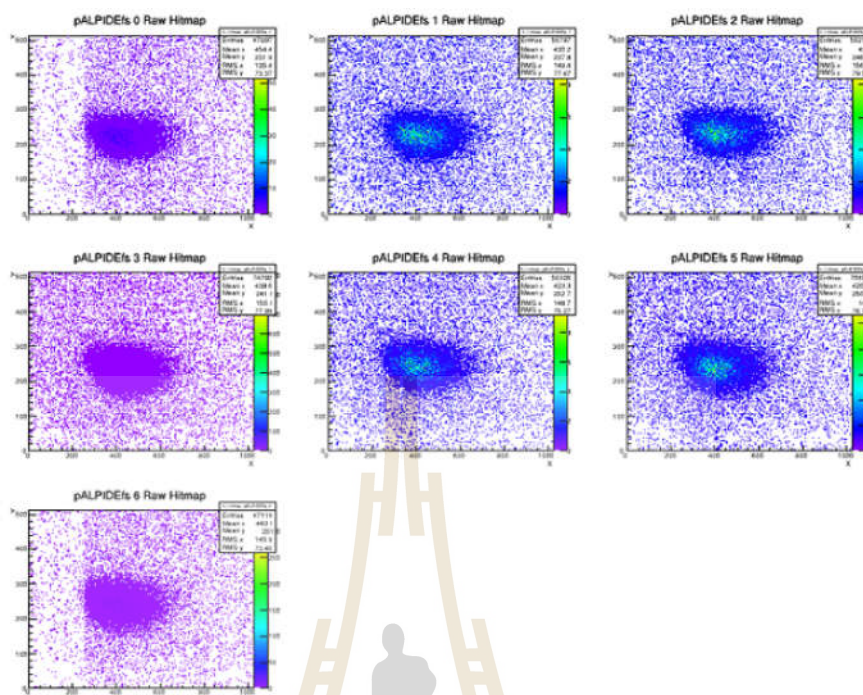


Figure A.5 An electron point beam profile.

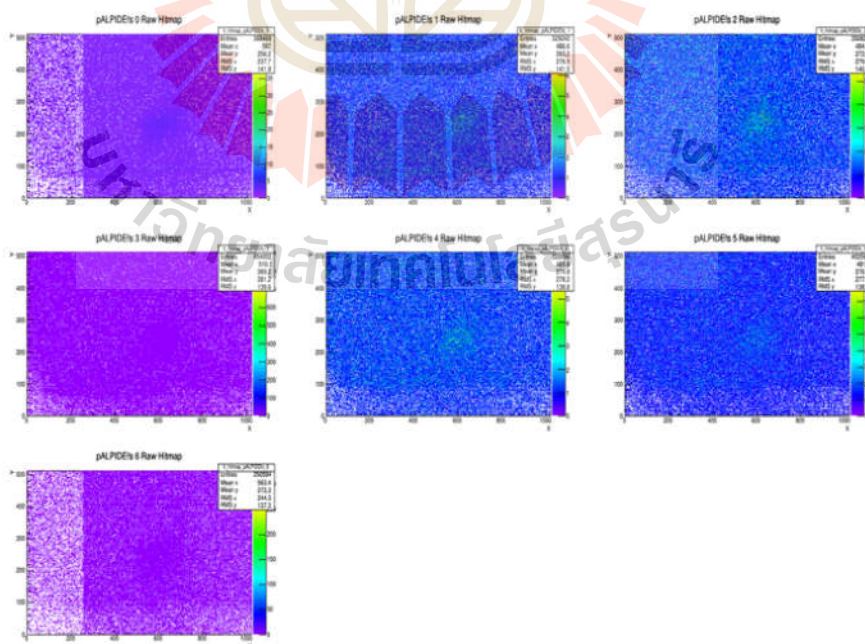


Figure A.6 An electron full beam profile.

Table A.3 Settings of High-energy Beam Transport(HBT) line magnet power supply for a full beam profile.

Symbol	Instruments	Current
	Description	(Amp.)
H-BV-M1	Bending vertical magnet power supply 1	0.0
H-BH-M1	Bending horizontal magnet power supply 1	84.39
H-BV-M2	Bending vertical magnet power supply 2	0.0
H-BH-M2	Bending horizontal magnet power supply 2	0.0
H-QD-M1	Quadrupole de-focus magnet power supply 1	15.0
H-QF-M2	Quadrupole focus magnet power supply 2	18.0
H-QD-M3	Quadrupole de-focus magnet power supply 3	9.5
H-QF-M4	Quadrupole focus magnet power supply 4	12.5
H-QF-M5	Quadrupole focus magnet power supply 5	0.0
H-QD-M6	Quadrupole de-focus magnet power supply 6	0.0
H-QF-M7	Quadrupole focus magnet power supply 7	0.0
H-QD-M8	Quadrupole de-focus magnet power supply 8	0.0
H-STV-M1	Steering vertical magnet power supply 1	14.0
H-STV-M2	Steering vertical magnet power supply 2	-11.0
H-STH-M3	Steering horizontal magnet power supply 3	-11.0
H-STV-M4	Steering vertical magnet power supply 4	1.0
H-STH-M5	Steering horizontal magnet power supply 5	0.0
H-STH-M6	Steering horizontal magnet power supply 6	0.0
H-STV-M7	Steering vertical magnet power supply 7	0.0

APPENDIX B

EXTENSION OF AN OPERATION

MANUSCRIPT FOR AN EUDAQ

FRAMEWORK

Configuration

EUDAQ data-taking configuration can be found on path `conf/palpidefs.conf` file. There are importance parameters (Grosse-Oetringhaus, 2014), which are

- `RunSizeLimit` (in Bytes): whenever the limit of the current file is reached, the run is automatically stopped and restarted a new run.
- `QueueSize` (in MB): the reserved memory area per detector layer to buffer an event, which is the event building, is slower than the acquiring events.
- `QueueFullDelay` (in ms): a period that system will pause in case the queue is full.
- `StatusInterval` (in s): the times of the chip temperatures period are read out and appeared in the data stream.
- `ReadoutMode`: The EUDAQ readout mode for card firmware correctness. There are 0 for event-based and 1 for packet-based readout. It must be the correct firmware on the card to support the selected mode.

- Devices: Number of DAQ boards which should be used for data-taking. For each of them needs to be their section. For example,

1. BoardAddress ID: DAQ board address where configured with jumpers on the debug pins 7:0

2. Noisy Pixel File ID (optional): The file which contains a list of noisy pixels that will be masked in the data-taking. The format of this file contains one pixel to be masked which is identified by

REGION DOUBLECOLUMN ADDRESS

This format is compatible with a file which is used in the TDAQboard class.

3. Chip Type ID: pALPIDE 1, 2, 3, or 4 determined by a chip which is a type of any chip in the position.

4. Config File ID (optional): configuration registers which are set after powering the chip. The configuration file is an XML file which can also be used with the crystal-ball tool. There is a tree structure following the composition of the register addresses. As shown as an example.

```
<?xml version="1.0"?>
<root>
  <address base="6">
    <address rgn="0">
      <address sub="1">
        <title>VCASN / VCASP</title>
        <value begin="0" width="8"><content>50</content></value>
        <value begin="8" width="8"><content>A0</content></value>
      </address> </address>
```

```
</address>
```

```
</root>
```

The number of a VCASN of 80 in a decimal number is needed to transform to be a hexadecimal number is 50 for configuration. Also, then VCASP of 160 in a decimal number is needed to transform to be a hexadecimal number A0.

EUDAQ restarting in case of trouble

During a data taking, if unknown debug or error from log collector appears, the problem can be immediately solved by restarting an EUDAQ as following procedure.

1. Investigating from the “log collector” window that config file was the last(error or debug) one or the “STARTRUN” tab of the shell.
2. Closing the remaining open EUDAQ windows
 - (a) go the shell window
 - (b) go to the “STARTRUN” tab and type command ./KILLRUN to automatic terminate an EUDAQ window.
3. Power cycle set up
 - go to the shell window
 - go to the “POWER” tab
 - execute power off.py to close power supply
 - execute power on.py to restart power supply
 - execute power status.py to check a status of an electric voltage and current

The voltages should be

- (a) Channel 1: 5 volts and 2 Amp. or more for main electric supply or cubic plug-in.
- (b) Channel 2: 3 volts and 0.3 mA ($<1\text{mA}$) for back-bias voltage in p-well lemo port.
- (c) Channel 3: 0V and 0.1 mA ($<15\text{mA}$) for No back bias voltage chip.

4. Starting the software

- (a) go to the shell window
- (b) go to the tab "STARTRUN" and type `./STARTRUN` to restart an EUDAQ window.
- (c) wait until all 4 windows are opened. there are run control, log collector, data collector and pALPIDEfs producer.
- (d) select a proper initial file and click "Init" button to download
- (e) select the last configuration file which didn't work and press the "Configure" button
- (f) wait until all producers are configured when colour turns green
- (g) press "START" to start the next run

5. Checking the data

- (a) go to the shell window
- (b) select the online-monitor tab by execute `./OnlineMon.exe -sc 0 -f ..data/run000xxx.raw` to open
- (c) check hitmaps and correlations

APPENDIX C

FUNCTIONAL TEST

A functional test is the electronic properties test for the prototype of ALPIDE sensor. This test is for checking and confirming the working conditions of the sensor before testing with a beam test. It can be separated into five processes.

1. First In First Out (FIFO): it is the first electronic communication test between each column and row of detector that contrast in 32 columns of a layer.
2. SCAN Digital-Analog (SCANDAC): it is a converter at the end of the peripheral circuit of each pixel.
3. Threshold scan is a measurement of electron level which separates a ratio between a noise and a real signal. The threshold level is determined from the configuration of a hexadecimal number which defines the lowest of hit signal current at sensing node.
4. Noise occupancy is a fake-hit scan on a chip. In this scanning, the fake-hit is investigated from an un-real hit from the noise signal detected by electronic scanning.

Basically, a noise occupancy is a study to find an un-real hit which occurs from a noise signal in term of a fake hit rate $[\text{pixel} \cdot \text{event}]^{-1}$ with a configuring variable. To study a noise occupancy on an ALPIDE chip. A dominant quantity in a discriminator is determined to split a signal from noise. There are, Threshold

current (I_{thre}), CASN voltage (V_{casn}) and back bias voltage. This study leads to the finding of an appropriated setting parameter. To find a good discriminator parameter, a fake hit rate is used to investigate the best setting. A fake hit rate should be lower than 10^{-5} [pixel · event] $^{-1}$ as an ITS upgrade requirement. A back-bias is applied to produced a built-in electric field for the depletion region. In principle, wider depletion region can reduce a collective charge in a Si-wafer and also reduce a noise perturbation from a collective charge. From the synthesis, a back-bias voltage is chosen to study the effect with noise-occupancy. By three parameters of a back-bias are defined to characterize. There are 0, -3 and -6 voltages of a back-bias voltage.

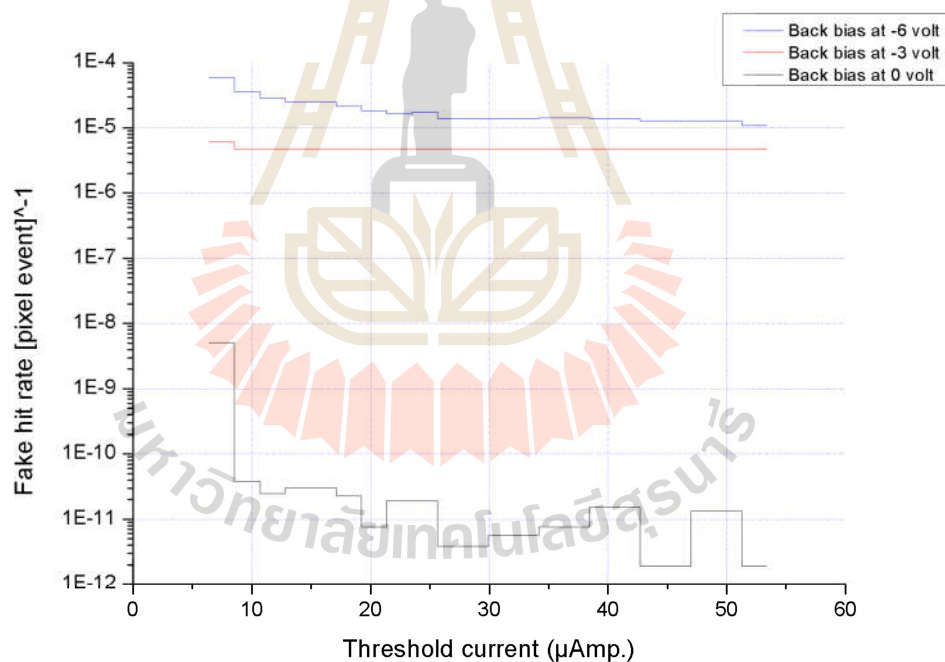


Figure C.1 a relation of threshold current(I_{thre}) with Fake hit rate [pixel · event] $^{-1}$ at 0, -3 , -6 back-bias voltage.

As shown in figure C.1, a trend of fake hit rate [pixel · event] $^{-1}$ decrease with increasing of a threshold current(I_{thre}) and decrease with increasing of a back-bias voltage. In figure C.2, C.3 and C.4 a trend of fake hit rate [pixel · event] $^{-1}$

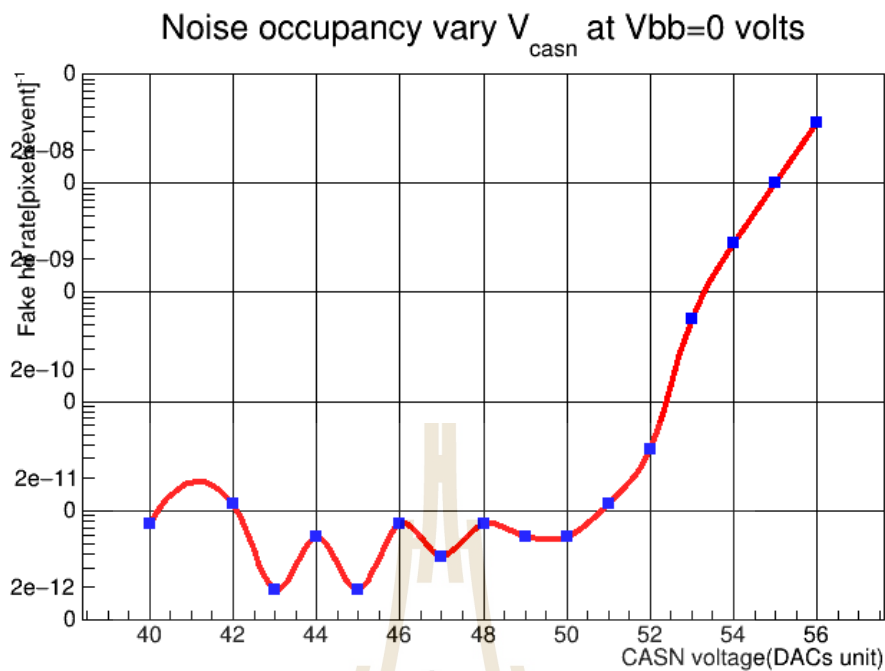


Figure C.2 a relation of a CASN voltage (V_{casn}) with Fake hit rate [pixel · event]⁻¹ at 0 back-bias voltage.

sharply increases with increasing of a CASN voltage (V_{casn}). In contrast, at -6 volts of a back bias voltage provides a fake hit rate over 10^{-5} [pixel · event]⁻¹. Hence -6 volts of a back bias voltage is not proper to set up as a parameter for working conditions.

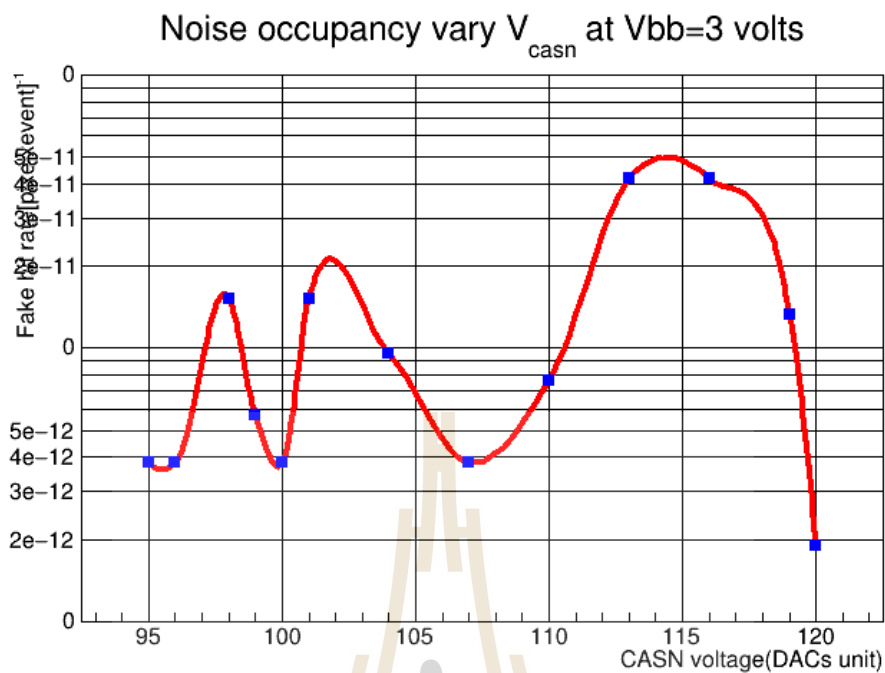


Figure C.3 a relation of a CASN voltage (V_{casn}) with Fake hit rate [pixel · event]⁻¹ at -3 back-bias voltage.

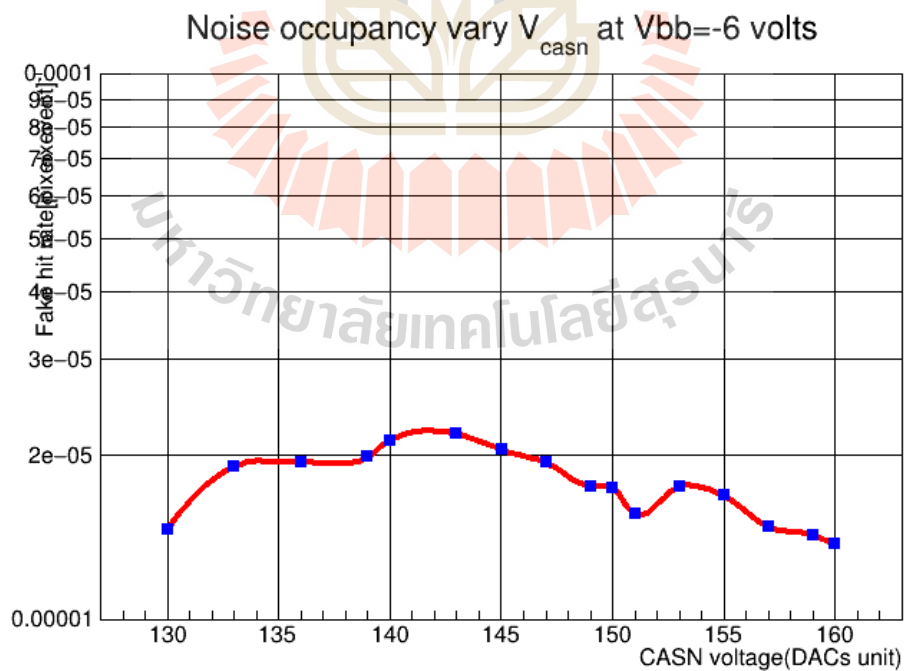


Figure C.4 a relation of a CASN voltage (V_{casn}) with Fake hit rate [pixel · event]⁻¹ at -6 back-bias voltage.

CURRICULUM VITAE

NAME: ANANTACHAI LAKRATHOK **GENDER:** Male

NATIONALITY: Thai

DATE OF BIRTH: MAY 14, 1993

E-MAIL: anantaon@mail.com

EDUCATIONS:

- 2005 - 2010, High school at Rajsima wittayalai school
- 2011 - 2014, Bachelor of Science, Physics department, Institute of science, Khonkaen University
- 2015 - 2019. Master of Science, School of Physics, Institute of Science, Suranaree University of Technology

PUBLICATIONS

1. A. Lakrathok, N. Laojamnongwong, N. Chanlek , K. Kittimanapun, and C. Kobdaj, School of Physics, Suranaree University of Technology and Synchrotron Light Research Institute (Public Organization), Thailand, Setup and commissioning of the test beam telescope for sensor characterization at the 1 GeV Test Beam at SLRI Beam Test Facility, The proceeding of the 7th International Graduate Research Conference (IGRC 7), Ubonratchatani University.
2. K. Kittimanapun, N. Chanlek, A. Lakrathok, and N. Laoiamnongwong, Low Intensity Electron Beam Measurement at SLRI Beam Test Facility, 9th International Particle Accelerator Conference, IPAC2018, Vancouver, BC, Canada, JACoW Publishing, ISBN: 978-3-95450-184-7, doi:10.18429/JACoW-IPAC2018-THPMK086.